ORIGINAL RESEARCH

Stress-Induced Cyclin C Translocation Regulates Cardiac Mitochondrial Dynamics

Jessica M. Ponce, PhD; Grace Coen, BS; Kathryn M. Spitler, PhD; Nikola Dragisic, MD; Ines Martins, BS;
Antentor Hinton Jr, PhD; Margaret Mungai, BS; Satya Murthy Tadinada, PhD; Hao Zhang, PhD;
Gavin Y. Oudit, MD, PhD; Long-Sheng Song, MD, MS; Na Li, PhD; Peter Sicinski, MD, PhD; Stefan Strack, PhD;
E. Dale Abel, MD, PhD; Colleen Mitchell, PhD; Duane D. Hall, PhD; Chad E. Grueter, PhD

BACKGROUND: Nuclear-to-mitochondrial communication regulating gene expression and mitochondrial function is a critical process following cardiac ischemic injury. In this study, we determined that cyclin C, a component of the Mediator complex, regulates cardiac and mitochondrial function in part by modifying mitochondrial fission. We tested the hypothesis that cyclin C functions as a transcriptional cofactor in the nucleus and a signaling molecule stimulating mitochondrial fission in response to stimuli such as cardiac ischemia.

METHODS AND RESULTS: We utilized gain- and loss-of-function mouse models in which the *CCNC* (cyclin C) gene was constitutively expressed (transgenic, CycC cTg) or deleted (knockout, CycC cKO) in cardiomyocytes. The knockout and transgenic mice exhibited decreased cardiac function and altered mitochondria morphology. The hearts of knockout mice had enlarged mitochondria with increased length and area, whereas mitochondria from the hearts of transgenic mice were significantly smaller, demonstrating a role for cyclin C in regulating mitochondrial dynamics in vivo. Hearts from knockout mice displayed altered gene transcription and metabolic function, suggesting that cyclin C is essential for maintaining normal cardiac function. In vitro and in vivo studies revealed that cyclin C translocates to the cytoplasm, enhancing mitochondria fission following stress. We demonstrated that cyclin C interacts with Cdk1 (cyclin-dependent kinase 1) in vivo following ischemia/reperfusion injury and that, consequently, pretreatment with a Cdk1 inhibitor results in reduced mitochondrial fission. This finding suggests a potential therapeutic target to regulate mitochondrial dynamics in response to stress.

CONCLUSIONS: Our study revealed that cyclin C acts as a nuclear-to-mitochondrial signaling factor that regulates both cardiac hypertrophic gene expression and mitochondrial fission. This finding provides new insights into the regulation of cardiac energy metabolism following acute ischemic injury.

Key Words: ischemia ∎ mitochondria ∎ signal transduction ∎ transcriptional coactivator ∎ transgenic mice

Cardiovascular disease (CVD) is the leading cause of morbidity and mortality in the United States, and risk factors include metabolic-related disease and genetic abnormalities.[1,2] Cyclin C is a component of Mediator, a large multisubunit complex that serves as a bridge between DNA-bound transcription factors and RNA polymerase II.[3] Alterations in the function of Mediator and the kinase submodule, which is composed of a Cdk8 (cyclin-dependent kinase 8), Med13 (mediator complex subunit 13), Med12, and cyclin C, have been correlated with congenital heart and CVD-related metabolic defects.[4–8] However, the involvement of cyclin C in cardiac function or metabolism has not been explored. Independent of its role in Mediator, cyclin C is a key component of stress-induced mitochondrial hyperfission in yeast and murine embryonic fibroblast.[9–13] In addition, studies have shown that osteosarcoma cultures display semifragmented mitochondria in the presence of constitutively cytoplasmic cyclin C.[13] However, the role of cyclin C in the mammalian heart in vivo is unknown.

CLINICAL PERSPECTIVE

What Is New?

- Mitochondrial fragmentation occurs in response to acute cardiac ischemic insult that is mediated in part through cyclin C translocation from the nucleus to augment fission.

What Are the Clinical Implications?

- Targeting this pathway to reduce mitochondria fragmentation may provide a therapeutic approach to reducing cardiomyocyte loss in ischemia.

Nonstandard Abbreviations and Acronyms

AAR	Area at risk
AAV	adeno-associated virus
cKO	conditional knockout
Cre	cre-recombinase
cTg	conditional transgenic
CVD	cardiovascular disease
Fl	floxed
I/R	ischemia reperfusion
MI	Myocardial Infarction
NRCM	neonatal rat cardiomyocyte
O2k	Oxygraph-2k (Oroboros Instruments)

The constant electrical and mechanical activities of the heart require a continuous energy supply met by a rich stockpile of mitochondria,[14] which maintain proper function by undergoing a constant cycle of fusion (ie, process of merging the double membrane of 2 mitochondria[13]) and fission (ie, process of mitochondrial division).[15–18] Mitochondria fission is a normal mechanism to maintain a population of healthy mitochondria; however, a dramatic increase in fission (hyperfission or fragmentation) can be detrimental to the cell.[19–22] Defects in the fission–fusion equilibrium result in mitochondrial autophagy (ie, mitophagy); cell necrosis; disrupted metabolic pathways; and, ultimately, cell death, leading to cardiomyopathies in mice.[15,21] Notably, in humans, mitochondrial dysfunction plays a role in the pathogenesis of CVD, including myocardial ischemia/reperfusion (I/R) injury.[23,24] However, the mechanistic relationship between mitochondria dynamics and CVD remains incompletely understood.

In this study, we have elucidated a role of cyclin C in transcription, mitochondrial dynamics, and CVD.

Using in vitro and in vivo models, we demonstrate that cyclin C regulates metabolic gene expression and mitochondrial dynamics in the murine heart in a manner dependent on its subcellular localization and that its disruption leads to cardiomyopathy and a decline in cardiac function. Furthermore, we showed that cyclin C interacts with Cdk1 in the cytoplasm following I/R injury and that mitochondrial hyperfission is reduced following Cdk1 inhibition. Together, these findings suggest that cyclin C regulates both hypertrophic gene expression and mitochondrial fission following myocardial ischemia and that inhibiting cyclin C cytoplasmic activity may provide a therapeutic approach to reduce ischemic damage.

METHODS

The RNA sequencing data are available at the National Center for Biotechnology Information (NCBI) Gene Expression Omnibus (GEO) database (accession No. GSE144947). Materials generated for the article are available on request. The supporting data are available within the article. Expanded methods are included as Data S1.

Mouse Models

Cardiomyocyte-specific cyclin C knockout mice were generated by breeding cyclin C floxed mice (CycC^{fl/fl}, kindly provided by Dr Peter Sicinski at Harvard University) with C57/BL6 transgenic mice containing the α-myosin heavy chain (αMHC) promoter-driven Cre recombinase to establish heterozygous cyclin C[fl/+]; αMHC Cre mice. Male cyclin C[fl/+]; αMHC Cre+ mice were bred to female cyclin C[fl/fl] mice to establish homozygous cyclin C fl/fl; αMHC Cre/+ (CycC cKO). Studies were done using Cre-negative cyclin C[fl/fl] littermates as controls.

Conditional cardiomyocyte-specific cyclin C–overexpressing mice were generated at the University of Iowa Genome Editing Facility by pronuclear injection of a linearized targeting vector into B6×SJL F2 pronuclei. The targeting construct was made by replacing the ZsGreen coding sequence of pCAG-loxPSTOPloxP-ZsGreen (Addgene 51269) with the coding region of *CCNC* (NCBI accession No. NM_005190) containing a C-terminal Myc tag. Founders were identified by genotyping with primers specific for the hGH polyA sequence downstream of *CCNC* (forward, 5′-GTCTATT CGGGAACCAAGCTGGAGT-3′; reverse, 5′-AACAGG CATCTACTGAGTGGACCCAA-3′) and backcrossed to C57BL/6 mice (Charles River Laboratories, strain code 027) for at least 5 generations for all studies. Cyclin C overexpression was induced through crossing loxPSTOPLoxP-*CCNC* (fl/+) mice with αMHC Cre–expressing mice (cyclin C cTg). Unless otherwise

stated, at least 3 CycC cTg and 3 cyclin C$^{fl/+}$ littermate control mice were used for all experiments. Similar results were obtained for male and female animals. Age-matched cyclin C fl/+;Cre negative and αMHCCre alone were used as controls. Animals were fed standard chow, and water was given ad libitum.

Human Explanted Heart Specimen Procurement

The human explanted heart samples were collected under the protocols approved by the Health Research Ethics Board of the University of Alberta. Signed consent and assent were obtained from individual participants (or next of kin) before cardiac transplantation or organ donation. Nonfailing myocardial specimens were procured from 5 consecutive donors with no cardiovascular history who were unsuitable for transplant because of medical or technical issues, such as ABO blood type incompatibility, as per the Human Organ Procurement and Exchange Program at the University of Alberta Hospital. Adult failing heart tissues were collected from patients with end-stage heart failure secondary to ischemic coronary artery diseases (n=6) as part of the Human Explanted Heart Program at the Mazankowski Alberta Heart Institute. The collections were conducted when the patients underwent cardiac transplantations, and all myocardium samples were excised from the post–myocardial infarction (MI) left ventricular free wall avoiding epicardial adipose tissue within 5 to 10 minutes of its excision following cold cardioplegia. The samples were immediately flash-frozen in liquid nitrogen and later stored in ultralow (−80°C) freezers. Detailed demographic and clinical profiles of all patients with coronary artery diseases are summarized in Table S1. The nonfailing control group consisted of 5 explanted hearts from men with a median age of 52 years (interquartile range: 38.0–54.0 years) and median left ventricular ejection fraction of 60% (interquartile range: 60–65%).

Cell Culture

To isolate primary cultures of neonatal rat cardiomyocyte (NRCM), hearts from P3 Wistar rats (Jackson Laboratory) were rapidly excised and washed in chilled Hanks Balanced Salt Solution (HBSS, 1X). The atria were removed, and ventricles were carefully minced and dissociated into single cells by proteolytic enzymes (Pierce Primary Cardiomyocyte Isolation Kit) dissolved in HBSS in a 37°C incubator for 30 to 35 minutes with gentle stirring. Enzymes were removed by washing cells 3 times with chilled HBSS. To break up tissue, cells were gently pipetted repeatedly with L-DMEM (M199; 10% horse serum, 5% fetal bovine serum, 1% penicillin). Cells were plated onto collagen-coated culture plates and allowed to adhere to the plates for 24 hours before changing to basic experimental culture DMEM (M199; 2% fetal bovine serum, 1% penicillin). NRCMs were stressed with angiotensin II (100 nmol/L), isoproterenol (200 nmol/L), or palmitate (50 μmol/L) 48 hours after seeding for varied durations. The culture medium was changed daily until the cells were harvested.

Adeno-Associated Virus Expression

Primary NRCMs were plated onto collagen-coated coverslips and maintained in modified DMEM culture (Pierce Primary Cardiomyocyte Isolation DMEM cell culture) medium for 24 hours. Cells were infected with adeno-associated virus (AAV; 5×10^7 vg/μL) expressing wild-type cyclin C, mutant cyclin C–holoenzyme-associated domain mutant (HAD), mutant cyclin C-ND (export domain), or control (empty vector control) for 72 hours. Adeno-associated vectors were generated by the University of Iowa Gene Vector Core Facility.

Cellular and Whole-Heart Lysate Fractionation

Following treatment, cells were collected, and fractionation was completed using the NE-PER Nuclear and Cytoplasmic Extraction Kit (Thermo), according the manufacturer's instructions. Cells and tissue were washed with chilled PBS and centrifuged at 500g for 5 minutes. Supernatant was discarded; cytoplasmic and nuclear proteins were extracted and stored at −80°C. Equal protein amounts from each fraction were analyzed by Western blotting.

Quantitative Real-Time Polymerase Chain Reaction

Ventricular tissue was isolated and flash frozen in liquid nitrogen and stored at −80°C until processed. Flash-frozen ventricles were pulverized with a Bessman tissue pulverizer before homogenization. Total RNA was extracted in TRIzol reagent (Invitrogen) using a Potter-Elvehjem tissue grinder. Reverse transcriptase polymerase chain reaction was performed to generate cDNA using SuperScript III (Invitrogen). For quantitative reverse transcriptase polymerase chain reaction, 50 ng of cDNA were used for each reaction with iTAQ Universal Sybergreen reagent (Bio-Rad), using the QuantStudio 6 Flex system (Applied Biosystems). Gene expression was analyzed using the $\Delta\Delta C_T$ method, and relative expression was normalized to Rpl7 l1. Sequences for the primers are as listed in previous studies.[6,8]

Immunofluorescence Microscopy

Isolated NRCMs were grown on collagen-coated glass coverslips. After treatment, cells were washed 3 times with PBS and fixed with ice-cold ethanol (100% v/v) for

15 minutes at room temperature. To suppress unspecific labeling, cells were incubated with blocking solution (1% BSA, 1% goat serum, and 0.1% Triton X-100 in PBS) for 1 hour at room temperature. Rabbit anti–cyclin C antibody (1:100), mitotracker orange (1:500) and phallodin-647 (1:400) in 1% BSA solution (in PBS, pH 7.4) were added for 1 hour at room temperature. After 3 washes with chilled PBS, the secondary antibodies conjugated with Alexa Fluor 488 or Alexa Fluor 568 (1:300) were added for 1 hour at room temperature. Cells were washed and mounted with Vectashield (Vectorlabs) containing DAPI for nuclear staining. Immunofluorescence was observed using a Zeiss 710 confocal microscope.

Immunohistochemical Staining

All samples were processed in consultation with the University of Iowa Central Microscopy Facility and Comparative Pathology core. Briefly, hearts were fixed in 4% paraformaldehyde, paraffin embedded, and sectioned (10 µm) using a standard microtome. Heart sections were deparaffinized and stained to determine changes in morphology (hematoxylin and eosin) or trichrome, as previously published.[6,8]

Immunoblot Analysis

Isolated NRCMs were removed from plates with 0.25% trypsin in a 37°C incubator for 3 to 5 minutes. Cells were washed twice with PBS and centrifuged at 30 000g for 10 minutes. Whole hearts were harvested and rinsed with chilled PBS. Ventricles were flash frozen and kept at –80°C until processing for total protein. Ventricular tissue was pulverized with a Bessman tissue pulverizer (Spectrum Labs) and homogenized in RIPA buffer (25 mmol/L Tris-HCl, pH 7.6, 150 mmol/L NaCl, 1% NP-40, 1% Na-deoxycholate, 0.1% SDS; Thermo Fisher Scientific) containing complete Mini protease and phosphatase inhibitors (Roche). Cells or tissue samples were sonicated on ice for 10 seconds with an ultrasonic liquid processor (Qsonica) and centrifuged at 20 000g at 4°C. Protein concentrations were determined by the bicinchoninic acid assay method (Thermo Fisher Scientific). Samples were separated for immunodetection using standard SDS-PAGE with 20 µg lysate per lane on 4% to 20% Tris-glycine SDS gels (Bio-Rad Laboratories) and transferred to 0.45-µm polyvinyl difluoride membranes (EMD Millipore). Membranes were blocked in blocking buffer (10 mmol/L Tris-HCl, pH7.4, 150 mmol/L NaCl, 0.05% Tween-20, 5% BSA or 5% nonfat dry milk), incubated in blocking buffer with primary antibodies overnight at 4°C, washed, and incubated with HRP-linked secondary antibodies (Jackson ImmunoResearch; at 1:10 000) for 1 hour at room temperature. Primary antibodies were used at the following dilutions: cyclin C (antirabbit, 1:2000 [Bethyl], 1:1000 [Thermo]), dynamin-related GTPase

(antirabbit, 1:500; Cell Signaling), phosphorylated Drp1 at serine 616, (pDrp) (antirabbit, 1:500; Cell Signaling). Glyceraldehyde 3-phosphate dehydrogenase (Gapdh) (1:8000; Cell Signaling), topo-isomerase (1:500; Cell Signaling), and RNA-pol II (1:10 000; Sigma Aldrich) were used as loading control.

Mitochondria Respiration Analysis

Complex activity was assessed using a Seahorse XF96 Extracellular Flux Analyzer by the University of Iowa Free Radical and Radiation Biology Research Core, following a previously established protocol.[25,26] NRCMs were isolated and plated at 40 000 cells per well in the XF96 plate format and treated with cyclin C-AAV for 72 hours. Plates were spun at 4°C at 2000g for 20 minutes to affix cells to the wells. The assay was run in the presence of 5 mmol/L pyruvate and 5 mmol/L malate, with sequential injections of FCCP (carbonilcyanide p-triflouromethoxyphenylhydrazone) and antimycin A to final concentrations of 4 µmol/L each. A minimum of 7 technical replicates were used for each cell isolation and treatment. The Oxygraph-2k (O2k; OROBOROS Instruments) was used for measurements of respiration and combined with the Fluorescence-Sensor Green of the O2k-Fluo LED2-Module for H_2O_2 measurement at the University of Iowa Metabolic Core. Two O2k instruments were used in parallel. Experiments using tissue homogenate and permeabilized cells were performed in MiR05 (110 mmol/L sucrose, 60 mmol/L K-lactobionate, 0.5 mmol/L EGTA, 3 mmol/L $MgCl_2$, 20 mmol/L taurine, 10 mmol/L KH_2PO_4, 20 mmol/L HEPES, pH 7.1 at 30°C, and 0.1% BSA essentially fatty acid free). DMEM supplemented with 10% fetal bovine serum and 50 U/mL penicillin and 50 µg/mL streptomycin was used for measurements on intact cells. All experiments were performed at 37°C. The medium was reoxygenated when oxygen concentrations reached 80 µmol/L.

MI Surgeries

MI induction was performed as described with minor modifications.[27] Briefly, we intubated and placed the mouse on a rodent miniventilator (Harvard Apparatus) connected to a Millennium oxygen concentrator apparatus (Respironics) that provided 94% to 98% oxygen. The ventilator was set at positive end-expiratory pressure mode of ventilation with a stroke volume of 200 Al and 200 strokes/min. The remaining surgery was performed using the method by Gao et al.[27] The skin was cut exposing the left pectoralis major muscles. The pectoralis muscles were then separated, and a small opening was made between the ribs; the heart was pulled through this opening, and a 10/0 Prolene suture (Ethicon; Johnson & Johnson) was then passed under the left anterior descending artery at ≈1 mm distal to the

left atrial appendage immediately after the bifurcation of major left coronary artery. The chest wall was closed by approximating the third and fourth ribs with 1 or 2 interrupted stitches using a 5/0 Chromic Catgut absorbable suture (Ethicon; Johnson & Johnson). Skin was closed with 6/0 Prolene continuous sutures. The mouse was gently disconnected from the ventilator, and spontaneous breathing usually resumed almost immediately.

I/R Surgeries

Ischemia induction was performed as described for the MI, with the following exceptions.[27] Following 20 minutes of ischemia, the knot in the suture occluding the left anterior descending artery was released to allow for reperfusion of the ischemic area and generation of I/R injury for 90 minutes. Next, the left anterior descending artery was religated, and 2% Evans blue was directly injected into aorta to observe ischemic and remote regions, which were immediately harvested.

Cardiac Function Analysis

To identify potential changes in gross cardiac morphology and markers of heart failure, body weight (in grams) and heart weight (ventricle and atria) and lung weight (in milligrams) were measured. To determine and evaluate the degree of infarction, we used triphenyl tetrazolium chloride staining on transverse heart sections. Sections were incubated in 1% triphenyl tetrazolium chloride in PBS for 20 minutes at 37°C and fixed in 10% formalin overnight. The samples were imaged using a Leica MZ 12 dissection scope. Cardiac function was evaluated in conscious mice in the University of Iowa Cardiology animal phenotyping core laboratory. Left-sided chest hair was removed. Parasternal long- and short-axis views were obtained using a high-frequency echocardiography (30 MHz) linear array transducer (Vevo 2100; VisualSonics). Measurements were performed by a single experienced operator blinded to the mouse genotypes.

RNA Sequencing Analysis

The University of Iowa Institute of Human Genetics, Genomics Division, generated polyA-enriched stranded RNA libraries followed by RNA sequencing (RNA-seq) using the Illumina HiSeq platform. Raw sequence reads were analyzed with BaseSpace (https://www.basespace.illumina.com/) by aligning reads to the Mus musculus mm10 genome using the TopHat Alignment app. Transcripts were assembled, and significant differentially expressed genes were determined with the Cufflinks Assembly and DE app using a false discovery rate <0.05. The RNA-seq analysis list of differentially regulated genes significantly changed between cyclin C fl/fl and cyclin C

cKO mouse hearts was entered into the PANTHER (protein analysis through evolutionary relationships) classification system (http://pantherdb.org/). Classification of data were compiled via biological process, and a pie chart was created. Alterations in biological processes pertaining to metabolic processes were performed to break down individual metabolic processes. RNA-seq analysis data were uploaded to Qiagen's Ingenuity pathway analysis, and biological and interaction networks were generated. The gene list was analyzed for biological function enrichment analysis, upstream regulator analysis, and networks of interaction between molecules algorithmically generated based on their connectivity.

High-Magnification Transmission Electron Microscopy

Jeol electron microscope (JEM-1230) was used at ×1500 to ×30 000 direct magnifications (Jeol) on 90-nm sections of fixed left ventricular tissue or area at risk (AAR) regions of sham or I/R-treated hearts. All samples were processed in consultation with the University of Iowa Central Microscopy Facility. Tissue was fixed in 2% glutaraldehyde and 2% paraformaldehyde in 0.1M buffer, dehydrated and embedded in resin bead capsules, and baked (70°C oven) for 24 hours. Tissue was sectioned (0.9-μm thickness; Leica UC6 Ultramicrotome II) on 300-μm mesh copper grids, stained using NaOH and lead citrate, and imaged. Mitochondrial size, area, and length were measured using ImageJ (National Institutes of Health) in a double-blind study. Analysis was performed using Matlab software. Briefly, mitochondrial length and area were binned, normalized to compute percentages, and then plotted via histogram. The mitochondria length and area were fit to a gamma distribution curve. Statistical analysis was performed on the binned data using Kruskal-Wallis test to detect changes in distribution.

Pharmacologic Studies

In in vitro analysis, isolated P3 NRCMs were treated with the Cdk1 inhibitor roscovitine (R7772; Sigma-Aldrich) at 5 μmol/L and 6-hour treatment and NU6102 (CAS 444722-95-6; Sigma-Aldrich) at 5 μmol/L and 6 hours. In in vivo analysis, roscovitine was solubilized in DMSO and diluted in 0.9% sodium chloride. Intraperitoneal injection of roscovitine was performed 1 hour before I/R surgery.

Coimmunoprecipitation

The AAR region of ventricular lysates was harvested from 8 to 10-week-old C57/bl-6 mice treated with sham or I/R surgeries and prepared using RIPA buffer with the addition of a protease phosphatase inhibitor cocktail

(Roche). Coimmunoprecipitation was performed using the Dynabead Protein A protocol (Thermo Fisher) and according to the manufacturer's instructions. Briefly, Dynabeads were prepared and bound to 10 µg of Cdk1 (Santa Cruz) or cyclin C antibody (Thermo) in 200 µL PBS with Tween-20 and then incubated for 20 minutes at room temperature. To the extracts, 5 µL of cyclin C (Thermo) or Cdk1 (Santa Cruz) antibody was added and incubated with gentle rotation for 2 hours at 4°C followed by the addition of 5 µL of Dynabeads Protein A (Invitrogen) with a further incubation of 1 to 2 hours. Immune complexes were washed, and target antigen was eluted and gently resuspended in NuPAGE 4X LDS Sample Buffer (Thermo) and NuPAGE 10X Sample Reducing Agent (Thermo) and detected via immunoblotting in the presence of cyclin C (Thermo) or Cdk1 (Santa Cruz) antibodies.

Statistical Analysis

Results are expressed as mean±standard error (S.E.). An unpaired Student *t* test was used to determine statistical significance of all samples with 2 groups, and ANOVA was performed for groups of ≥3 with a Tukey correction using GraphPad Prism (GraphPad Software). Significance was defined as $P<0.05$ unless indicated otherwise within the figure legend. The raw mitochondria length and area data for each experiment were for fit to a γ-distribution curve. Statistical analysis was performed on the binned data using the Kruskal–Wallis test, a nonparametric test to compare the groups representing to detect changes in distribution.

Study Approval

All animal experimental procedures were approved by the University of Iowa Animal Care and Use Committee. All experiments using human samples were performed with written informed consent received from patients before inclusion in this study and in accordance with the institutional guidelines and were approved by the institutional ethics committee.

RESULTS

Cardiac Cyclin C Expression Is Sufficient to Alter Cardiac Function and Mitochondrial Dynamics

Protein levels for several components of Mediator including the kinase submodule are increased in models of heart disease, suggesting a role in regulating crucial cardiac gene expression and maintenance of heart function in response to stress.[5,6,8,28] In the developing mouse heart, cyclin C expression

was highly expressed from birth to postnatal day 14. Expression decreased at postnatal day 21 into adulthood (Figure S1A). A common feature of a heart under a variety of pathophysiologic conditions is the postnatal switch back to the "fetal" gene program, including components of Mediator as an adaptive mechanism.[29] To determine whether expression of cyclin C is also altered in the context of heart disease, we assessed cyclin C expression levels in infarct, peri-infarct, and noninfarct regions of ischemic and healthy human hearts. Cyclin C expression in human ischemic heart disease is highly variable (Figure 1A, Table S1). To determine whether cyclin C translocation from the nucleus to the cytoplasm observed on oxidative stress in yeast is conserved in murine hearts under cardiac stress, we evaluated cyclin C localization in C57/Bl6 8 to 10-week-old male mouse hearts following I/R surgeries. We found increased cytoplasmic cyclin C levels in the remote and AAR regions compared with sham surgical controls (Figure 1B). Together, these data demonstrate that cyclin C translocation from the nucleus to the cytoplasm does occur in the mammalian heart following I/R injury.

To investigate whether the cyclin C acts as a protective adaptation to cardiac stress or could represent a direct pathophysiologic mechanism, we generated transgenic mice that conditionally overexpress *Ccnc* in cardiomyocytes when coexpressed with Cre recombinase driven by the *Myh6* promoter (CycC *c*Tg; Figure 1C). Assessments of 3-week-old mice show overexpression of cyclin C protein levels in ventricular tissue (Figure 1D). CycC *c*Tg hearts do not display gross morphologic changes (Figure 1E, Figure S1B); however, a statistically significant increase in end-systolic function and significant decline in ejection fraction demonstrates a negative effect of cyclin C overexpression on cardiac function (Figure 1E). Histologic evaluation demonstrated normal muscle morphology, and no changes were detected in collagen deposition using Masson's trichrome staining (Figure S1C).

Because cyclin C overexpression has been shown to drive mitochondrial fragmentation in mouse embryonic fibroblasts,[9,13] we wanted to explore the effects of cyclin C cardiac-specific overexpression on mitochondria in cardiomyocytes. To determine whether the increased expression of cyclin C affected mitochondria morphology in the context of cardiac stress, we also performed MI surgeries on CycC *c*Tg and CycC^{fl/+} control mice and assessed mitochondria morphology 48 hours following surgery in the underperfused AAR of the myocardium that is limited to circulation during an MI[7] (Figure S1D and S1E). Transmission electron microscopy analysis of left ventricles revealed that CycC *c*Tg mice have increased mitochondria disarray
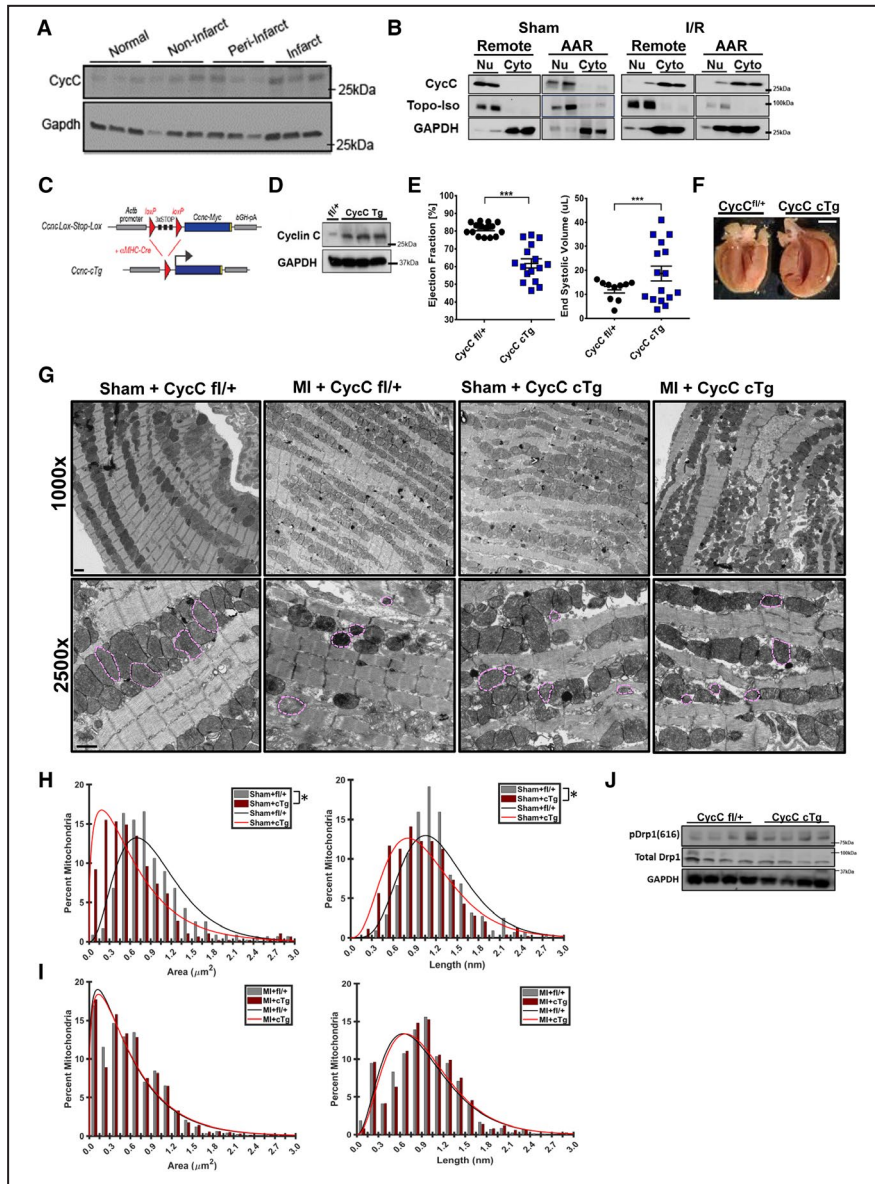
Figure 1. Cyclin C (CycC) expression is increased in human and murine heart disease, resulting in altered mitochondrial morphology.
A, Immunoblot of CycC and Gapdh control in healthy, infarcted, peri-infarcted, and noninfarcted regions of human ventricular tissue samples from patients (n=3). **B**, Immunoblot of CycC, topo-isomerase (Topo-Iso), and Gapdh in nuclear (Nu) and cytoplasmic (Cyto) fractionated tissue from 8- to 10-week-old C57Bl/6 murine hearts following ischemia/reperfusion surgery (n=2). The area at risk (AAR) is a myocardial zone limited to circulation during an myocardial infarction (MI) that is underperfused and becomes necrotic rapidly. In sham surgeries, the AAR is tissue extracted from the left ventricle and below location of suture pass. **C**, Schematic of the inducible CycC transgenic targeting construct. Cre-mediated excision of the loxP-flanked Stop cassette enables transcription of Myc-tagged human *CCNC.* **D**, Immunoblot of CycC and Gapdh in ventricular tissue of CycC^fl/+ mice and cardiac-specific overexpression of CycC (CycC cTg; n=3). **E**, Anatomical images of hearts from CycC^fl/+ and CycC cTg mice. Scale bar=2.5 μm. **F**, Echocardiography analysis for end-systolic volume and ejection fraction in CycC^fl/+ and CycC cTg mice (15 per group). *P<0.05 compared with CycC^fl/+ mice. (**G**) TEM images of left ventricles of CycC^fl/+ and CycC cTg mice 72 hours following sham or MI surgeries (scale bar=2 μm [×1000], 0.5 μm [×2500]). **H** and **I**, Morphometric analysis of transmission electron microscopy images in (**G**) for mitochondrial length (**H**) and area (**I**). Lengths and area were binned, x-axis labels bin value for each bin range. *P<0.05; Kruskal–Wallis test by ranks and Student *t* test compared with genotype and sham controls. Gamma distribution curves (n=4; ≥500 mitochondria per group). **J**, Immunoblot of phosphorylated Drp1(616), total Drp1, and Gapdh protein expression levels in whole ventricular tissue of CycC^fl/+ and CycC cTg mice.

and fragmentation (Figure 1G, mitochondria outlined in pink). CycC cTg cardiac mitochondrial were significantly smaller in length and area compared with floxed controls (Figure 1H and 1I). CycC cTg hearts treated with MI injury displayed abnormal mitochondrial cristae, increased mitochondrial number, and significantly decreased mitochondrial length and area compared with CycC^{fl/+} mice or sham controls (Figure 1G through 1I). Importantly, the observed mitochondrial morphology shifts in CycC cTg hearts (Figure 1H) parallels the shift observed in MI-induced injury (Figure 1I, Figure S1G), illustrating that overexpression of cyclin C is sufficient to prompt alterations in mitochondrial form. In addition, we assessed levels of the phosphorylated dynamin-related GTPase Drp1 at site serine 616 (pDrp1[616]) as a biochemical marker of activated Drp1. We did not observe significant alterations in pDrp1(616) levels in CycC cTg mice versus wild-type controls (Figure 1J). These data demonstrate that overexpression of cyclin C in the heart is sufficient to alter mitochondrial integrity and can have profound effects on mitochondrial dynamics.

Cyclin C Deficiency Results in Declined Cardiac and Mitochondria Function With Altered Gene Transcription

To determine whether cyclin C is necessary for normal function in the murine heart, we generated mice with cardiac-specific deletion in the *Ccnc* gene (Cyc C cKO) by crossing cyclin C floxed mice (*Cyc^{fl/fl}*) to transgenic mice expressing Cre recombinase under a constitutively active cardiomyocyte-specific αMHC promoter. Three-week-old Cyc C cKO hearts have a significant reduction in *Ccnc* mRNA expression and a loss of cyclin C protein compared with mice expressing the cyC homozygous floxed allele (in the absence of Cre recombinase (ie, cyc C[fl/fl]; Figure 2A and 2B). Notably, analysis of 12-week-old hearts by echocardiography revealed significantly increased heart mass (66%) in Cyc C cKO hearts compared with Cyc C[fl/fl] (Figure 2C and 2D). A significant increase of heart and lung mass was also observed in 20-week-old mice (Figure S2A). Histologic analysis displayed no distinct changes in tissue morphology (Figure S2B). We next determined whether these differences translated to functional defects. Echocardiography analysis depicted a significant increase in left ventricular mass, end-diastolic function, end-systolic function, and a reduction in both heart rate and ejection fraction in Cyc C cKO mice when compared with sex- and age-matched 12-week-old Cyc C[fl/fl] controls (Figure 2D). Thus, cardiac-specific deletion illustrates that cyclin C is necessary for normal cardiac morphology and function.

Cyclin C binds to and activates cyclin-dependent kinase Cdk8 to regulate gene transcription.[6,30–32]

Therefore, to assess the transcriptional profile of cyclin C–deficient hearts, we performed RNA-seq analysis on 6-week-old ventricles from Cyc C[fl/fl] and Cyc C cKO mice. In the absence of cyclin C, 336 genes were differentially regulated (173 downregulated, 163 upregulated, false-discovery rate <0.05; Figure 2E, GEO accession number GSE144947). KEGG (Kyoto Encyclopedia of Genes and Genomes) pathway analysis revealed that genes involved in PPAR (peroxisome proliferator–activated receptor) signaling pathways (*Pck1, Plin1, Plin5, Acadm, DBI, Slc27a1*), FoxO signaling pathways (*Rag1*), and AMPK signaling pathways (*Adipoq, Scd1*) were all significantly downregulated. Interestingly, adult-expressed genes related to hypertrophic and dilated cardiomyopathy (*Myl2, Ryr2, Tnni3, Tnnt1, Tnnc1*), muscle contraction (*Itga7, Cacnad1*), and adrenergic signaling in cardiomyocytes (*Adra1b, Cacna2d1*) were also downregulated in Cyc C cKO hearts (Figure 2F). These data corroborate the phenotypic observations of altered cardiac morphology and function observed in 12-week-old mice. To assess alterations in molecular function, Ingenuity pathway analysis results depicted genes involved in metabolic-related processes (*Pkig, Cdo1, Srpk3, Rgs2, Ces1d*) and mitochondria function (*Dbi, Idh3b, Pck1, Ndufa5, Cdo1, Ogdhl, Ndufa13, Me3, Maob, Akr1b10*) as significantly misregulated (Figure 2G). Validation of RNA-seq analysis of 6-week-old hearts via quantitative reverse transcriptase polymerase chain reaction demonstrates upregulation of hypertrophic markers (*Nppb, Acta1, Tnni1*) and downregulation of genes related to mitochondrial function *(Cox5*; Figure S2C–S2E). In further analysis of the RNA-seq data sets to assess potential differences in upstream transcriptional regulatory regions, several predicted promoter transcriptional factor motifs were also enriched that are involved in metabolism (Hnf4), development and differentiation (Hen1, Foxo1, Nfe2, MyoD, Mef2, Pax4), and tumorigenesis (Tal1, Tcf3, Tef1; Figure S2F). These data demonstrate an explicit role of cyclin C as a transcriptional cofactor in regulating genes involved in cardiac metabolism and function.

The altered gene expression prompted us to evaluate Cyc C cKO regulation of cardiac metabolism by assessing oxygen flux and mitochondrial morphology. High-resolution respiratory analysis of 12-week-old Cyc C cKO and control cardiac septum tissue was performed using saturating concentrations of ADP and substrates for complex I (malate, pyruvate, glutamate), β-oxidation (palmitoyl-L-carnitine), and complex II (succinate). Relative to CycO^{fl/fl} hearts, CycC cKO cardiac tissue displayed a significant decrease in oxygen consumption in the presence of glutamate. Cyclin C–depleted hearts also demonstrated significantly decreased palmitoyl-carnitine/malate–supported oxygen flux and a significant decline in ADP-driven mitochondrial oxygen consumption following treatment
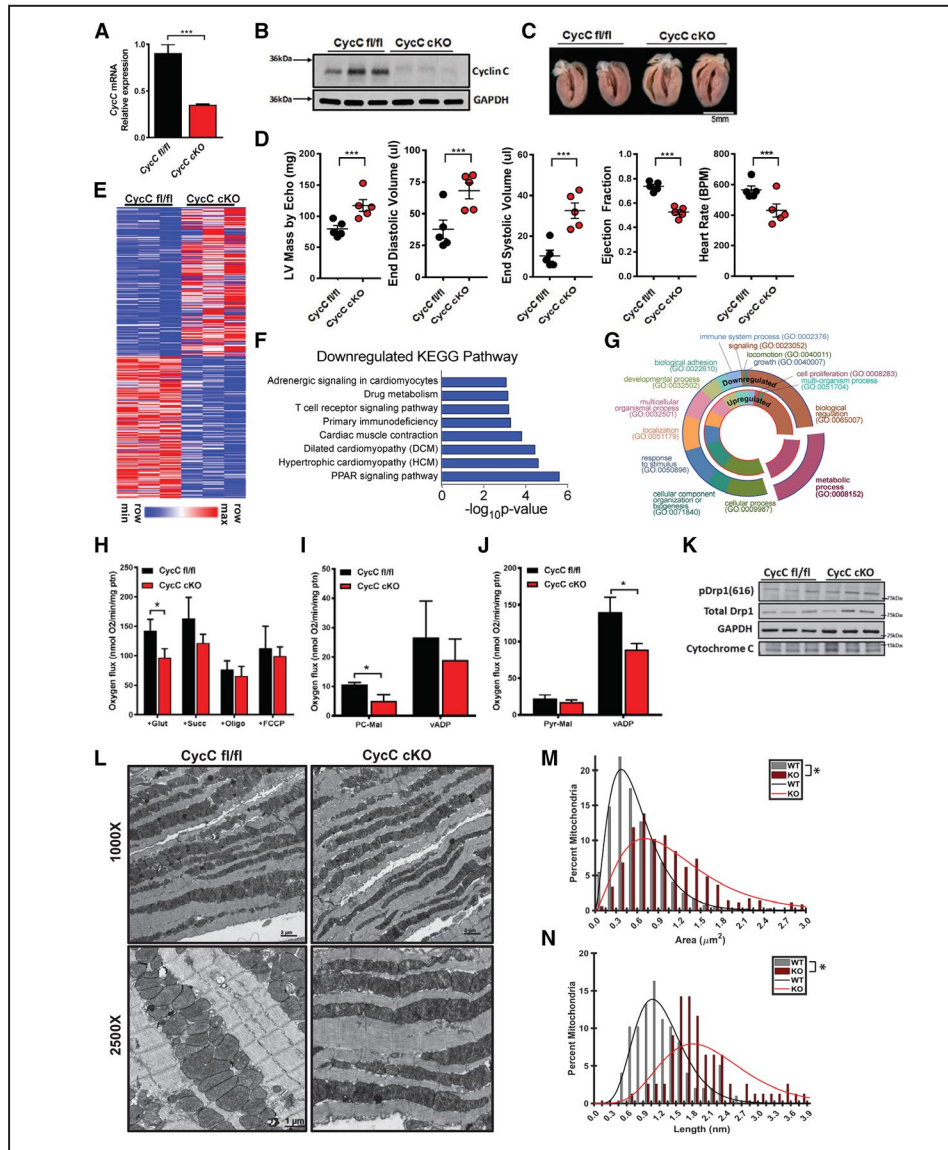
Figure 2. Cardiac-specific deletion of cyclin C (CycC) induces pathologic heart defects associated with altered gene expression and mitochondria function.

Quantitative reverse transcriptase polymerase chain reaction (**A**) and immunoblot analysis (**B**) of CycC expression in ventricular tissue from 3-week-old cardiac-specific knockout mice (CycC cKO) or littermate controls (CycC$^{fl/fl}$). Data are mean±SEM (n=3); *$P<0.05$ vs controls. **C**, Anatomical cardiac image from 12-week-old CycC$^{fl/fl}$ or CycC cKO mice. **D**, Echocardiography analysis for left ventricular (LV) mass, end-diastolic volume, end-systolic volume, ejection fraction, and heart rate in 12-week-old CycC$^{fl/fl}$ or CycC cKO mice (n=12); *$P<0.05$ vs controls. **E**, Heat map displaying RNA sequencing results in 6-week-old CycC$^{fl/fl}$ or CycC cKO ventricular tissue indicating relative gene expression values for differentially expressed genes with >5 fragments per kilobase per million reads (n=3). **F**, KEGG pathway analysis of downregulated genes in ventricular tissue of 6-week old CycC$^{fl/fl}$ relative to CycC cKO mice. **G**, Gene ontology term enrichment for significant up- and downregulated differentially expressed genes. **H** through **J**, High-resolution respirometry analysis measuring oxygen flux in saponin-permeabilized cardiac fibers from 12-week-old murine hearts. Glutamate and succinate (**H**), palmitoyl-carnitine (PC)–malate and ADP (2 mmol/L) (**I**), and pyrimidine-malate (**J**) were used as substrates, with oligomycin inhibitor and FCCP (carbonilcyanide p-tri flouromethoxyphenylhydrazone) uncoupler (*$P<0.05$ for genotype). Data are expressed as mean±SEM, n=3. *$P<0.05$ vs CycC$^{fl/fl}$ littermate controls. (**K**) Immunoblot analysis of phosphorylated Drp1(616), total Drp1, and Gapdh protein expression levels in CycC$^{fl/+}$ and CycC cKO ventricular tissue. **L**, Representative transmission electron microscopy (TEM) images of LV tissue obtained from 12-week-old CycC$^{fl/fl}$ or CycC cKO mice (scale bar=2 μm [×1000], 0.5 μm [×2500]). **M** and **N**, Population distribution of cardiac mitochondrial length (**M**) and area (**N**) from TEM images in (**L**) using similar binning methods as Figure 1H–1L. *$P<0.05$; Kruskal–Wallis test and Student t test compared with genotype controls. Gamma distribution curves of the length and area (≥750 mitochondria per group). BPM indicates beats per minute.

with pyruvate-malate (Figure 2H–2J). These data demonstrate how cyclin C is necessary to maintain normal cardiac mitochondrial function. To determine alteration in mitochondrial fission machinery, we measured pDrp1(616) levels in Cyc C cKO and control hearts by Western blot and found no statistical difference (Figure 2K). Analysis of mitochondrial morphology via transmission electron microscopy showed that Cyc C cKO mitochondrial dynamics also appeared disrupted (Figure 2L, mitochondria outlined in pink). In contrast to the fragmented morphology observed in Cyc cTg mice, Cyc cKO hearts have larger, elongated mitochondria with a significantly increased area compared with Cyc C fl/fl hearts (Figure 2L–2N). Together, these data provide evidence that cyclin C plays a role in mitochondrial function and dynamics.

Cyclin C Localization Alters Mitochondrial Dynamics and Function in the Mammalian Heart

Following I/R injury, we found increased cyclin C in cytoplasmic fractions of whole-heart lysates (Figure 1B). This enticed us to investigate whether cyclin C localization regulates mitochondria morphology in cardiomyocytes. First, we analyzed cyclin C expression patterns in neonatal rat ventricular cardiomyocytes isolated from wild-type pups on postnatal day 3. Because translocation of nuclear proteins can depend on stress type, a variety of stimuli were tested. These included palmitate, a free fatty acid that induces oxidative stress; angiotensin II, the main effector molecule of the renin–angiotensin system known to contribute to the development and progression of heart failure; isoproterenol, a catecholamine known to induce cardiac hypertrophy by mimicking sustained adrenergic stimulation; and phenylephrine, a hypertrophic α_1-adrenoceptor agonist.[33–36]

Following treatment with palmitate, angiotensin II, phenylephrine, and isoproterenol, cytoplasmic levels of cyclin C significantly increased, as determined by immunofluorescence and cell fractionation with Western blotting for palmitate and angiotensin II treatments in NRCMs and adult rat cardiomyocytes (Figure 3A–3C, Figure S3A). These data show that multiple established cardiovascular stress models induce the translocation of nuclear cyclin C to the cytoplasm in mammalian cardiomyocytes.

During cardiac stress, mitochondrial fission is increased, resulting in fragmented mitochondria.[16,17,37] To determine whether localization of cyclin C affected mitochondrial morphology, we generated AVVs that expressed full-length wild-type or mutated variants of cyclin C under the control of the cardiac troponin (*Tnnt2*) promoter. Neonatal rat ventricular cardiomyocytes transduced with cyclin C–holoenzyme-associated domain mutant (HAD),

which disrupts binding to Cdk8 and expels cyclin C to the cytoplasm,[14] show a significant decrease in mitochondrial length and form factor (indicative of mitochondrial fragmentation) and a significant increase in mitochondria number (Figure 3D and 3E, Figure S3B and S3C). Conversely, expression of the cyclin C-ND AAV, in which the export domain is mutated retaining cyclin C in the nucleus,[14] results in significantly increased mitochondrial length, decreased mitochondrial number, and increased form factor, indicative of mitochondrial elongation (Figure 3D and 3E, Figure S3B and S3C). This altered morphology suggests that cyclin C subcellular localization regulates mitochondrial fission/fusion dynamics in cardiomyocytes. We found a significant increase in pDrp1(616) in cells transduced with cytoplasmic cyclin C-HAD, as reflected by the increased mitochondria puncta (Figure 3F). Thus, these data demonstrate that the localization of cyclin C regulates mitochondrial fission in mammalian cardiomyocytes. Because both fission and fusion are crucial for proper mitochondrial function, cellular oxygen consumption rates in cells transduced with wild-type or mutant forms of cyclin C were evaluated by Seahorse analysis. Transduction of wild-type and mutant cyclin C decreased basal respiration, ATP-linked respiration, maximal respiratory capacity, and reserve capacity compared with cells transduced with AAVs encoding the control vector alone (Figure 3G–3K). Notably, the cytoplasmic mutant, cyclin C-HAD, presents a further significant decline in maximal respiratory capacity and a complete loss of oxygen consumption rate reserve capacity compared with wild-type and ND mutant cyclin C expression. These data suggest that cytoplasmic localization of cyclin C is sufficient to induce mitochondrial fission and dramatically repress mitochondrial function.

Effects of Cytoplasmic Cyclin C on Mitochondrial Dynamics Are Reduced by the Cdk1 Inhibitor

It is well established that I/R injury leads to increased mitochondrial fission; however, the molecular mechanism by which this occurs is still not completely understood.[21,24,38,39] Studies demonstrate that controlling Drp1 activation by inhibiting phosphorylation at Ser616 can reduce mitochondrial fission during I/R injury in the heart.[21] Recent evidence suggests that Cdk1 activates mitochondrial fission in cardiomyocytes following anoxia-reoxygenation via phosphorylation of Drp1(616).[40] Because we have shown that cyclin C initiates hyperfission in cardiomyocytes, we propose that this process involves cyclin C, which is known to bind and activate Cdk1 in T-cell acute lymphoblastic leukemia cells.[41]
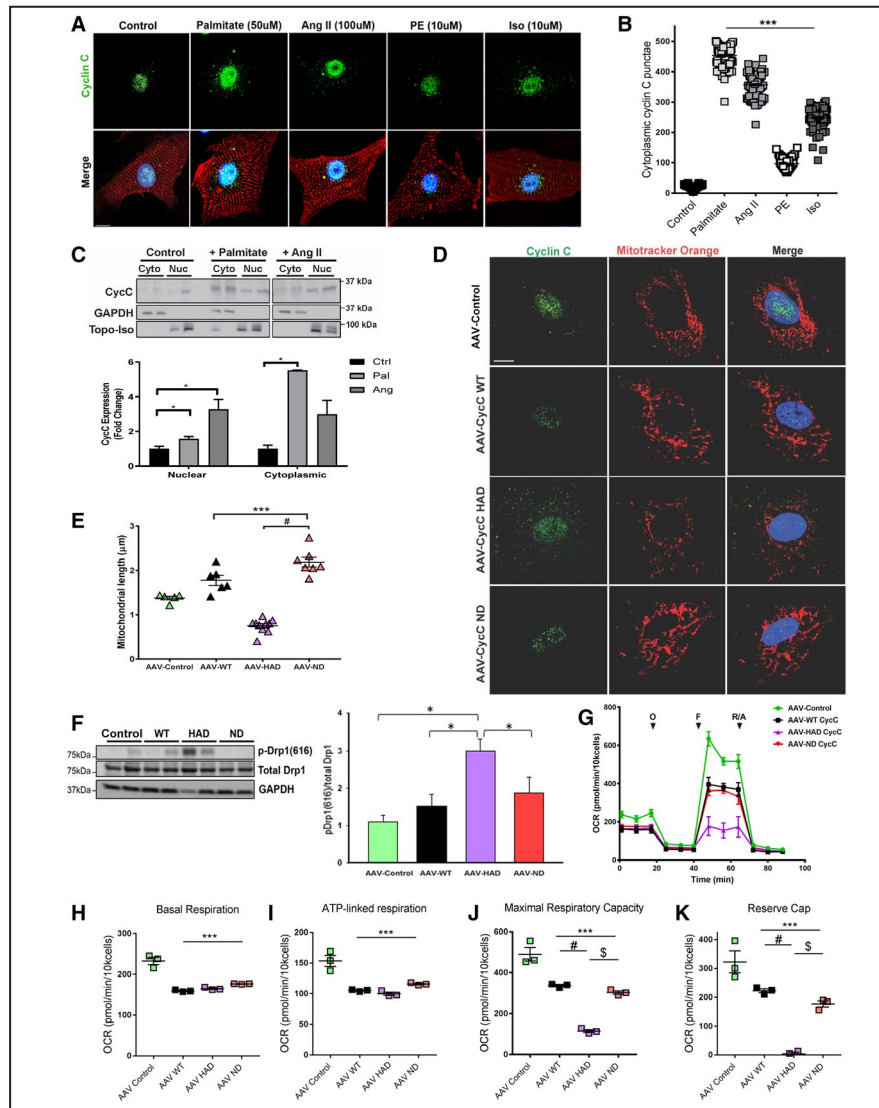
Figure 3. Stress-dependent translocation of cyclin C (CycC) from the nucleus to the cytoplasm regulates mitochondria hyperfission and function in neonatal rat cardiomyocytes (NRCMs).

(**A**) Immunofluorescence (IF) analysis of CycC (green) from postoperative day 3 (P3) NRCMs following treatment with palmitate (50 μmol/L, 15 minutes), angiotensin II (100 nmol/L, 30 minutes), phenylephrine (PE; 10 μmol/L, 1 hour), and isoproterenol (Iso; 10 μmol/L, 1 hour). Nuclei are stained with DAPI (blue). **B**, Quantification of cytoplasmic CycC puncti following 15 minutes of palmitate (50 μmol/L) and 30 minutes of angiotensin II (Ang II; 100 μmol/L), PE (10 μmol/L), and isoproterenol (10 μmol/L). *$^{***}P$<0.01 for all groups relative to control; ≥500 cells counted, 5 per group. **C**, Immunoblots of CycC, Gapdh, or topo-isomerase in fractionated NRCMs after treatment with palmitate (50 μmol/L, 15 minutes) or Ang II (100 nmol/L, 30 minutes). **D**, IF of NRCMs following transduction with adeno-associated virus (AAV)–expressing Myc-tagger wild-type and mutant CycC within its holoenzyme-associated domain (HAD) or export domain (ND). Localization of CycC (green) and mitochondrial morphology (red) were assessed using Mitotracker Orange 72 hours after AAV transduction. **E**, Quantification of mitochondrial length in NRCMs using the ImageJ processing program. *P<0.01; *$^{**}P$>0.05 for all groups relative to control; ANOVA, ≥500 cells counted, n=6. **F**, Immunoblot of AAV-transduced NRCMs treated as in (**E**) for phosphorylated Drp1(616) and total Drp1 (n=3). **G**, Mitochondrial respiration measurements obtained by Seahorse analysis in NRCMs treated as in (**D**). Arrows indicate the time points for administration of the corresponding inhibitors; 7 per group. **H** through **K**, Quantification of basal respiration, maximum respiratory capacity, ATP-linked respiration, and reserve capacity of NRMCs from (**I**), *$^{**}P$<0.05 for all groups relative to control cells treated with AAV-control. Scale bar=5 μm. F indicates FCCP; O, oligomycin; and R/A, rotenone/antimycin mix.
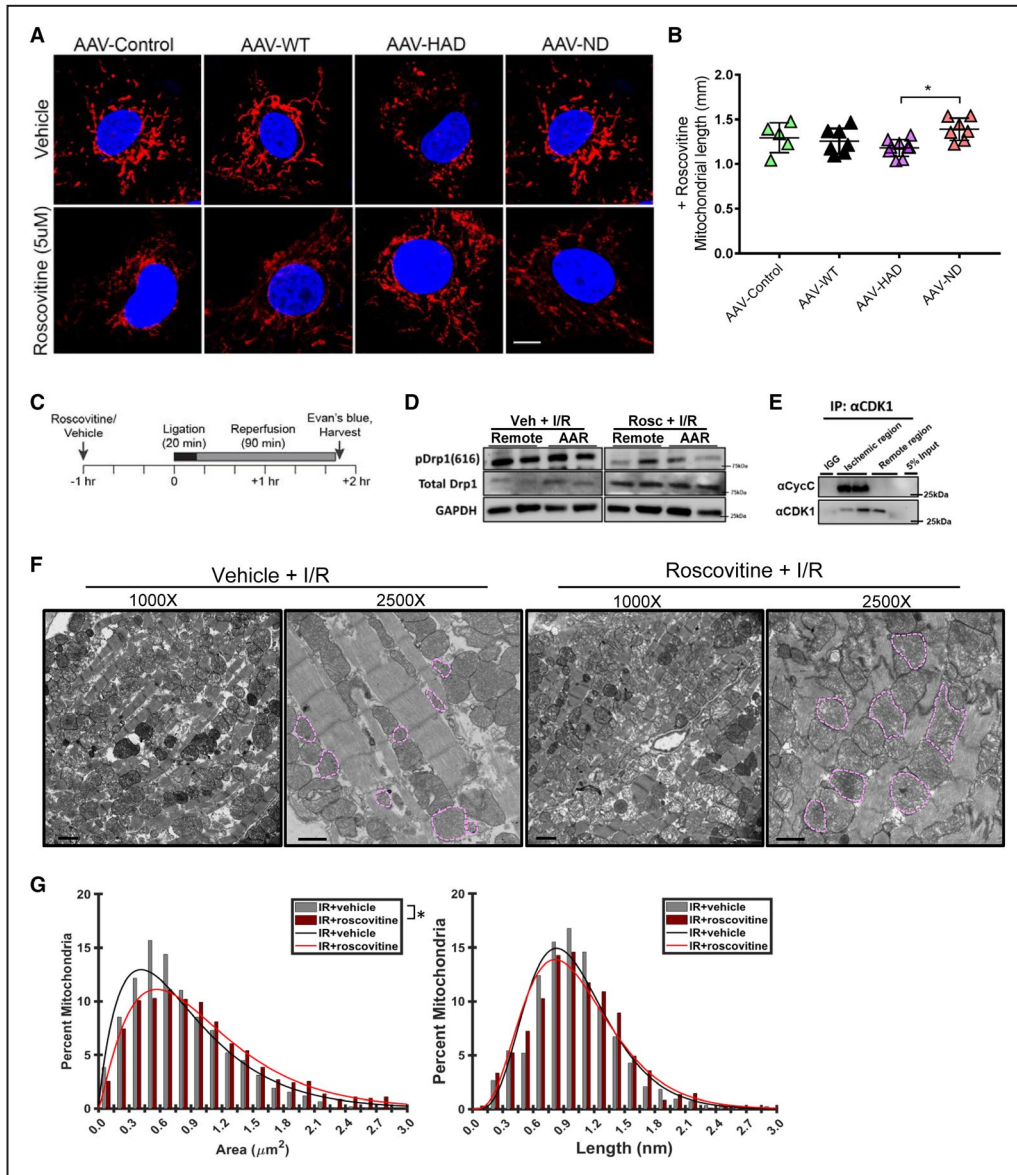
Figure 4. Cdk1 (cyclin-dependent kinase 1)–specific inhibitor alleviates cyclin C (CycC)–induced mitochondrial fission in vitro and in vivo.
A, Immunofluorescence of NRCMs transduced with adeno-associated virus (AAV)–expressing wild-type CycC (AAV-CycC WT), CycC–holoenzyme-associated domain (AAV-CycC HAD), CycC–export domain (AAV-CycC ND), or vector control (AAV-Control) in the presence or absence of roscovitine inhibitor (Rosc, 5 μmol/L, 1 hour). Mitochondrial morphology (red) is determined using Mitotracker orange (200 nmol/L). Scale bar=5 μm. **B**, Length of mitochondria in NRCMs transduced and treated as in (a) and quantified using ImageJ. *$^{***}P$>0.05; ANOVA, ≥500 cells counted, 5 per group. **C**, Outline of ischemia/reperfusion (I/R) protocol. Eight to 10-week-old C57BL/6 male mice were treated with Rosc or vehicle control (intraperitoneal injection) 1 hour before I/R surgery (3 mice per treatment; 2 in western blot). Following 20 minutes of ischemia, the ligature was removed, and hearts were reperfused for 90 minutes. Ischemic and remote regions were harvested for immediate subcellular fractionation processing (3 hearts per treatment; 2 shown). **D**, Immunoblot detecting CycC, pDrp1(616) (phosphorylated Dynamin-related GTPase), and total Drp expression in wild-type mice treated with Rosc or vehicle control following sham or I/R surgery, as outlined in (C). **E**, Coimmunoprecipitation of CycC:Cdk1 in cardiac ventricles from wild-type following I/R surgery, as outlined in (C). C57/BL6 male mice, 8–10 weeks old; 2 of 3 are shown. **F**, Representative transmission electron microscopy analysis on left ventricles of mouse hearts treated with vehicle or Rosc following I/R surgery (scale bar=2 μm [×1000], 0.5 μm [×2500]). **G**, Population distribution of cardiac mitochondrial area from ventricular tissue of C57Bl/6 mice following I/R stress and treated with Rosc or vehicle control. Gamma distribution curves representing the length and area (3 hearts per group; ≥850 mitochondria per heart). AAR indicates area at risk.

To determine whether cyclin C and Cdk1 regulate mitochondrial fission, we transduced NRCMs with cyclin C-AAVs for 72 hours and subsequently treated the cells with the Cdk1 inhibitor roscovitine for 24 hours. Following treatment with roscovitine, we observed elongated mitochondria in all AAV-treated NRCMs compared with those treated with vehicle controls (Figure 4A and 4B). This was a stark contrast to the fragmented mitochondria observed following treatment with cytoplasmic cyclin C-HAD virus alone (Figure 4A). To confirm specificity of Cdk1 inhibition, we performed similar immunofluorescence analysis on NRCMs treated with cyclin C-AAVs in the presence of a second Cdk1 inhibitor (NU6102; Abcam) and found similar elongated mitochondrial tubules observed with roscovitine treatment (Figure S3E). These data demonstrate that inhibiting Cdk1 activity can blunt cytoplasmic cyclin C–induced mitochondrial fission.

To determine the effects of inhibiting Cdk1 in vivo, we pretreated 8- to 10 week-old C57BL/6J males with roscovitine for 1 hour before performing I/R or sham surgeries (Figure 4C). No difference in pDrp1(616) levels was observed in mouse hearts with I/R injury and treated with vehicle control, whereas those treated with roscovitine showed decreased levels of pDrp1(616) (Figure 4D). This finding indicates that roscovitine can inhibit Cdk1-dependent phosphorylation of Drp1(616) in the heart.

Activation of Cdk1 requires the binding of specific cyclins.[27–29] Because cyclin C has been shown to bind and activate Cdk1 in tumor cells, we next determined whether cyclin C interacts with Cdk1 following I/R injury.[28] Thus, we immunoprecipitated Cdk1 from ventricular lysates isolated from AAR and remote regions of hearts following I/R injury or sham control and immunoblotted for cyclin C. Cyclin C-Cdk1 interacts in the ischemic region of left ventricle following I/R injury, suggesting that cyclin C initiates mitochondria fission via Cdk1 activation of Drp1 in the context of cardiac stress (Figure 4E). Finally, we performed transmission electron microscopy to assess inhibition of Cdk1 on mitochondrial morphology following I/R in wild-type mice. On inhibition of Cdk1 with roscovitine, we observed significant a increase in mitochondrial area with a trend for increased length compared with those from mice injected with vehicle controls (Figure 4F and 4G, mitochondria outlined in pink). Overall, these data suggest cytosolic cyclin C inhibition as a potential mechanism to protect against I/R injury.

DISCUSSION

Altered gene expression and mitochondrial dysfunction are two major contributors to the progression of CVD, including ischemic heart disease.[2,42] As a component of the Mediator kinase subunit in the nucleus, cyclin C binds and activates Cdk8 to regulate transcription[6,30]; however, our work illustrates an additional role of cyclin C in regulating cardiac mitochondrial dynamics. Notably, as in vivo cancer models have been utilized to investigate regulation of mammalian cyclin C,[41] the function of cyclin C in the heart has remained unexplored. The results of this study demonstrate how cyclin C plays a role independent of Mediator by regulating mitochondrial dynamics in the murine heart in vivo.

Oxidative stress is a causative factor in the pathophysiology of I/R injury.[37,43] In correlation with previous in vitro work using oxidative stress to stimulate cyclin C translocation,[9,10] we found that cytoplasmic cyclin C is elevated in hearts from mice from I/R injury compared with normal hearts. To differentiate the role of cyclin C as either a protective adaptation to cardiac stress or a propathophysiologic factor, we generated mouse models that overexpressed or depleted cyclin C in the mouse heart.

Our studies show that varying expression levels of cyclin C in cardiac tissue give rise to cardiac dysfunction and alterations in mitochondrial dynamics. Similar to expression patterns of other components of the Mediator kinase subunit,[4,6,28] we found that cyclin C expression in the mouse heart is elevated throughout development from embryonic day 18.5 through postnatal day 21 and decreases in adult cardiac tissue. Previous studies have shown Mediator protein expression to also increase during cardiac stress, indicating fetal-gene reprogramming in diseased hearts.[6,8,29] Other studies have also implicated Mediator kinase subunit components to be critical for cardiac function.[4,7,28,44–48] Mutations in Med13 alter transcriptional pathways in cardiomyocytes, and overexpression of Cdk8 induces eccentric ventricular hypertrophy, systolic dysfunction, and heart failure.[5,6,28] These results are consistent with those presented in this article, that depleting cyclin C alters transcription, specifically in pathways related to metabolism, cardiac muscle contraction, cardiomyopathy, and the citrate cycle. We also found predicted enrichment for altered upstream transcription factor activity involved in muscle development and disease. Based on these data, we propose that cyclin C is required for normal cardiac development and function.

The heart is a highly metabolically active organ, possessing the highest content of mitochondria of any tissue to supply its constant electrical and mechanical demands.[14] To maintain efficient function, a balance between mitochondrial fusion and fission must be met. Alterations in this process result in mitochondrial dysfunction associated with the development of numerous cardiac diseases such I/R

injury, cardiac hypertrophy and heart failure.[2,38,39,49] Specifically, previous studies have shown that conditional cardiomyocyte-specific knockout of Drp1 resulted in mitochondrial enlargement and lethal dilated cardiomyopathy, whereas conditional knockout of cardiomyocyte mitofusins caused mitochondrial fragmentation with eccentric remodeling, illustrating the importance of balancing mitochondrial dynamics.[16,50] Similarly, our studies show that altered expression of cyclin C (either its absence or overexpression) in the heart results in cardiac remodeling and contrasting mitochondrial morphology in mice. We found that cardiac-specific deletion of cyclin C resulted in elongated mitochondria that exhibited increased length and area, in addition to a declined metabolic function, suggesting that cyclin C is necessary for normal mitochondria function in murine hearts. Conversely, cyclin C overexpression in cardiac myocytes causes decreased area and mitochondria length, indicative of increased fission versus fusion dynamics similar to those observed in ischemic regions of hearts following MI. These findings suggest that expression levels of cyclin C may act as a rheostat to regulate mitochondrial dynamics during cardiac stress.

Studies in yeast show that oxidative stress prompts cyclin C translocation and induction of mitochondria hyperfission and regulated cell death.[9,10] Similarly, we found that cyclin C translocates from the nucleus to the cytoplasm in response to a variety of stresses in NRCMs and adult rodent cardiomyocytes. Using AAV viruses to express full-length or mutant forms of cyclin C in NRCMs, we found opposing effects on mitochondrial morphology, depending on cyclin C localization. Cells expressing cytoplasm-restricted cyclin C resulted in smaller, punctate mitochondria; cells expressing nuclear-retained cyclin C had longer mitochondria, demonstrating a change in mitochondrial dynamics. Consistent with previous studies showing a decline in mitochondria function on misregulation of fission machinery,[34] we showed that mitochondrial respiration is also dependent on the localization of cyclin C in cardiomyocytes. Thus, our results are the first to determine that cyclin C regulates mitochondrial fission machinery and function in the mammalian heart.

Because mitochondrial fission and fusion play critical roles in preserving mitochondrial homeostasis, disruption of these dynamics leads to cardiac disease, including ischemic injury.[21,39] Mitochondrial fission is mediated by Drp1, which, when phosphorylated at serine 616, oligomerizes to constrict and sever the mitochondrial membrane through a GTP hydrolysis-dependent mechanism.[15] Cyclin C activates various kinases in multiple cell types.[31,51] Defined as a class II cyclin that functions as a transcription factor,[10] cyclin C routinely forms a regulatory subcomplex with the nuclear kinase Cdk8; however, cyclin C has also been implicated as a haplo-insufficient tumor suppressor by activating Cdk19 and Cdk3[41] and drives cell proliferation through interactions with related kinases Cdk1 and Cdk2.[52] Because cyclin C interacts with Cdk1 in cancer cells, we investigated its potential role in Cdk1-dependent phosphorylation of Drp1(616).[40] Our studies are the first to show that cyclin C–Cdk1 interaction occurs following I/R injury in the murine heart. We also found that mitochondrial dynamics are likely shifted toward fusion after inhibiting Cdk1 or deleting cyclin C in the heart, whereas fission is favored under conditions of cyclin C cardiac–specific overexpression and nuclear exclusion suggesting cyclin C plays an important role in activating the mitochondria-fission related pathway. This work suggests cyclin C and Cdk1 are potential therapeutic targets in treating myocardial I/R injury by targeting their function as upstream regulators of mitochondria dynamics.

The rapid response to the changing electrical and mechanical demands of cardiomyocytes requires continuous crosstalk between the nucleus and mitochondria to ensure a constant energy supply. Cardiac injury activates multiple signaling mechanisms that alter nuclear transcription and mitochondrial structure and function.[1,17] Observing cardiac defects and imbalanced mitochondrial dynamics when cyclin C is absent or overproduced suggests its role as a mitochondrial–nuclear signal to maintain cellular equilibrium. Based on our studies, we propose that under basal conditions, nuclear cyclin C regulates gene transcription via the Mediator kinase submodule; however, on response to cardiac stress, cyclin C disbands from the kinase submodule, thereby allowing transcriptional activation of stress-response genes while concomitantly translocating to the cytoplasm to induce mitochondrial fission via Cdk1 activation and phosphorylation of Drp1(616). Thus, understanding the role of cyclin C as both a key transcriptional cofactor and regulator of mitochondrial integrity and function can potentially provide a new clinically relevant pathway to target for preserving of cardiac function following ischemic stress.

ARTICLE INFORMATION

Affiliations

From the Abboud Cardiovascular Research Center, Division of Cardiovascular Medicine, Department of Internal Medicine, Carver College of Medicine (J.M.P., G.C., I.M., A.H., M.M., L.-S.S., E.D.A., D.D.H., C.E.G.), Interdisciplinary Graduate Program in Genetics (J.M.P., C.E.G.), Department of Biochemistry, Carver College of Medicine (K.M.S.), Stead Family Department of Pediatrics (N.D.), Fraternal Order of Eagles Diabetes Research Center, Division of Endocrinology and Metabolism, Carver College of Medicine (A.H., M.M., L.-S.S., E.D.A., C.E.G.), Department of Pharmacology and Iowa Neuroscience Institute, Carver College of Medicine (S.M.T., S.S.), and Department of Mathematics and Delta Center (C.M.), University of Iowa, Iowa City, IA; Mazankowski Alberta Heart Institute Canada Research Chair in Heart Failure, Division of Cardiology, 2C2 Walter Mackenzie Health Sciences Centre Edmonton, Alberta, Canada (H.Z., G.Y.O.); Iowa City Veterans Affairs

Medical Center, Iowa City, IA (L.-S.S.); Department of Cancer Biology, Dana-Farber Cancer Institute, Boston, MA (N.L., P.S.); Department of Genetics, Harvard Medical School, Boston, MA (N.L., P.S.).

Disclosures

None.

Supplementary Materials

Data S1
Table S1
Figures S1–S3

REFERENCES

1. Kathiresan S, Srivastava D. Genetics of human cardiovascular disease. *Cell*. 2012;148:1242–1257.
2. Nan J, Zhu W, Rahman MS, Liu M, Li D, Su S, Zhang N, Hu X, Yu H, Gupta MP, et al. Molecular regulation of mitochondrial dynamics in cardiac disease. *Biochim Biophys Acta Mol Cell Res*. 2017;1864:1260–1273.
3. Allen BL, Taatjes DJ. The mediator complex: a central integrator of transcription. *Nat Rev Mol Cell Biol*. 2015;16:155–166.
4. Baskin KK, Makarewich CA, DeLeon SM, Ye W, Chen B, Beetz N, Schrewe H, Bassel-Duby R, Olson EN. Med12 regulates a transcriptional network of calcium-handling genes in the heart. *JCI Insight*. 2017;2:e91920.
5. Grueter CE, van Rooij E, Johnson BA, DeLeon SM, Sutherland LB, Qi X, Gautron L, Elmquist JK, Bassel-Duby R, Olson EN. A cardiac microrna governs systemic energy homeostasis by regulation of MED13. *Cell*. 2012;149:671–683.
6. Hall DD, Ponce JM, Chen B, Spitler KM, Alexia A, Oudit GY, Song LS, Grueter CE. Ectopic expression of Cdk8 induces eccentric hypertrophy and heart failure. *JCI insight*. 2017;2:e92476.
7. Hall DD, Spitler KM, Grueter CE. Disruption of cardiac Med1 inhibits RNA polymerase II promoter occupancy and promotes chromatin remodeling. *Am J Physiol Heart Circ Physiol*. 2019;316:H314–H325.
8. Spitler KM, Ponce JM, Oudit GY, Hall DD, Grueter CE. Cardiac Med1 deletion promotes early lethality, cardiac remodeling, and transcriptional reprogramming. *Am J Physiol Heart Circ Physiol*. 2017;312:H768–H780.
9. Cooper KF, Khakhina S, Kim SK, Strich R. Stress-induced nuclear-to-cytoplasmic translocation of cyclin C promotes mitochondrial fission in yeast. *Dev Cell*. 2014;28:161–173.
10. Ganesan V, Willis SD, Chang KT, Beluch S, Cooper KF, Strich R. Cyclin C directly stimulates Drp1 GTP affinity to mediate stress-induced mitochondrial hyperfission. *Mol Biol Cell*. 2019;30:302–311.
11. Jin C, Strich R, Cooper KF. Slt2p phosphorylation induces cyclin C nuclear-to-cytoplasmic translocation in response to oxidative stress. *Mol Biol Cell*. 2014;25:1396–1407.
12. Strich R, Cooper KF. The dual role of cyclin C connects stress regulated gene expression to mitochondrial dynamics. *Microb Cell*. 2014;1:318–324.
13. Wang K, Yan R, Cooper KF, Strich R. Cyclin C mediates stress-induced mitochondrial fission and apoptosis. *Mol Biol Cell*. 2015;26:1030–1043.
14. Chaanine AH, Joyce LD, Stulak JM, Maltais S, Joyce DL, Dearani JA, Klaus K, Nair KS, Hajjar RJ, Redfield MM. Mitochondrial morphology, dynamics, and function in human pressure overload or ischemic heart disease with preserved or reduced ejection fraction. *Circ Heart Fail*. 2019;12:e005131.
15. Chang CR, Blackstone C. Dynamic regulation of mitochondrial fission through modification of the dynamin-related protein Drp1. *Ann N Y Acad Sci*. 2010;1201:34–39.
16. Dorn GW II, Vega RB, Kelly DP. Mitochondrial biogenesis and dynamics in the developing and diseased heart. *Genes Dev*. 2015;29:1981–1991.
17. Iglewski M, Hill JA, Lavandero S, Rothermel BA. Mitochondrial fission and autophagy in the normal and diseased heart. *Curr Hypertens Rep*. 2010;12:418–425.
18. Song M, Gong G, Burelle Y, Gustafsson AB, Kitsis RN, Matkovich SJ, Dorn GW II. Interdependence of parkin-mediated mitophagy and mitochondrial fission in adult mouse hearts. *Circ Res*. 2015;117:346–351.
19. Brand CS, Tan VP, Brown JH, Miyamoto S. Rhoa regulates Drp1 mediated mitochondrial fission through rock to protect cardiomyocytes. *Cell Signal*. 2018;50:48–57.
20. Cribbs JT, Strack S. Reversible phosphorylation of Drp1 by cyclic amp-dependent protein kinase and calcineurin regulates mitochondrial fission and cell death. *EMBO Rep*. 2007;8:939–944.
21. Disatnik MH, Ferreira JC, Campos JC, Gomes KS, Dourado PM, Qi X, Mochly-Rosen D. Acute inhibition of excessive mitochondrial fission after myocardial infarction prevents long-term cardiac dysfunction. *J Am Heart Assoc*. 2013;2:e000461. 10.1161/JAHA.113.000461.
22. Frank S, Gaume B, Bergmann-Leitner ES, Leitner WW, Robert EG, Catez F, Smith CL, Youle RJ. The role of dynamin-related protein 1, a mediator of mitochondrial fission, in apoptosis. *Dev Cell*. 2001;1:515–525.
23. Inserte J, Hernando V, Garcia-Dorado D. Contribution of calpains to myocardial ischaemia/reperfusion injury. *Cardiovasc Res*. 2012;96:23–31.
24. Kalogeris T, Baines CP, Krenz M, Korthuis RJ. Cell biology of ischemia/reperfusion injury. *Int Rev Cell Mol Biol*. 2012;298:229–317.
25. Pereira RO, Tadinada SM, Zasadny FM, Oliveira KJ, Pires KMP, Olvera A, Jeffers J, Souvenir R, McGlauflin R, Seei A, et al. OPA1 deficiency promotes secretion of FGF21 from muscle that prevents obesity and insulin resistance. *EMBO J*. 2017;36:2126–2145.
26. Anderson EJ, Kypson AP, Rodriguez E, Anderson CA, Lehr EJ, Neufer PD. Substrate-specific derangements in mitochondrial metabolism and redox balance in the atrium of the type 2 diabetic human heart. *J Am Coll Cardiol*. 2009;54:1891–1898.
27. Gao E, Lei YH, Shang X, Huang ZM, Zuo L, Boucher M, Fan Q, Chuprun JK, Ma XL, Koch WJ. A novel and efficient model of coronary artery ligation and myocardial infarction in the mouse. *Circ Res*. 2010;107:1445–1453.
28. Baskin KK, Grueter CE, Kusminski CM, Holland WL, Bookout AL, Satapati S, Kong YM, Burgess SC, Malloy CR, Scherer PE, et al. Med13-dependent signaling from the heart confers leanness by enhancing metabolism in adipose tissue and liver. *EMBO Mol Med*. 2014;6:1610–1621.
29. Razeghi P, Young ME, Alcorn JL, Moravec CS, Frazier OH, Taegtmeyer H. Metabolic gene expression in fetal and failing human heart. *Circulation*. 2001;104:2923–2931.
30. Akoulitchev S, Chuikov S, Reinberg D. TFIIH is negatively regulated by CDK8-containing mediator complexes. *Nature*. 2000;407:102–106.

31. Barette C, Jariel-Encontre I, Piechaczyk M, Piette J. Human cyclin C protein is stabilized by its associated kinase CDK8, independently of its catalytic activity. *Oncogene*. 2001;20:551–562.

32. Belakavadi M, Fondell JD. Cyclin-dependent kinase 8 positively cooperates with mediator to promote thyroid hormone receptor-dependent transcriptional activation. *Mol Cell Biol*. 2010;30:2437–2448.

33. Wikstrom JD, Israeli T, Bachar-Wikstrom E, Swisa A, Ariav Y, Waiss M, Kaganovich D, Dor Y, Cerasi E, Leibowitz G. Ampk regulates er morphology and function in stressed pancreatic beta-cells via phosphorylation of Drp1. *Mol Endocrinol*. 2013;27:1706–1723.

34. Tsushima K, Bugger H, Wende AR, Soto J, Jenson GA, Tor AR, McGlauflin R, Kenny HC, Zhang Y, Souvenir R, et al. Mitochondrial reactive oxygen species in lipotoxic hearts induce post-translational modifications of AKAP121, Drp1, and OPA1 that promote mitochondrial fission. *Circ Res*. 2018;122:58–73.

35. Zhuo XZ, Wu Y, Ni YJ, Liu JH, Gong M, Wang XH, Wei F, Wang TZ, Yuan Z, Ma AQ, et al. Isoproterenol instigates cardiomyocyte apoptosis and heart failure via AMPK inactivation-mediated endoplasmic reticulum stress. *Apoptosis*. 2013;18:800–810.

36. Watkins SJ, Borthwick GM, Oakenfull R, Robson A, Arthur HM. Angiotensin II-induced cardiomyocyte hypertrophy in vitro is TAK1-dependent and Smad2/3-independent. *Hypertens Res*. 2012;35:393–398.

37. Chou CH, Lin CC, Yang MC, Wei CC, Liao HD, Lin RC, Tu WY, Kao TC, Hsu CM, Cheng JT, et al. GSK3beta-mediated Drp1 phosphorylation induced elongated mitochondrial morphology against oxidative stress. *PLoS One*. 2012;7:e49112.

38. Elsasser A, Suzuki K, Schaper J. Unresolved issues regarding the role of apoptosis in the pathogenesis of ischemic injury and heart failure. *J Mol Cell Cardiol*. 2000;32:711–724.

39. Ong SB, Subrayan S, Lim SY, Yellon DM, Davidson SM, Hausenloy DJ. Inhibiting mitochondrial fission protects the heart against ischemia/reperfusion injury. *Circulation*. 2010;121:2012–2022.

40. Zaja I, Bai X, Liu Y, Kikuchi C, Dosenovic S, Yan Y, Canfield SG, Bosnjak ZJ. CDK1, pkcdelta and calcineurin-mediated Drp1 pathway contributes to mitochondrial fission-induced cardiomyocyte death. *Biochem Biophys Res Commun*. 2014;453:710–721.

41. Li N, Fassl A, Chick J, Inuzuka H, Li X, Mansour MR, Liu L, Wang H, King B, Shaik S, et al. Cyclin c is a haploinsufficient tumour suppressor. *Nat Cell Biol*. 2014;16:1080–1091.

42. Meyers DE, Basha HI, Koenig MK. Mitochondrial cardiomyopathy: pathophysiology, diagnosis, and management. *Tex Heart Inst J*. 2013;40:385–394.

43. Patil N, Chavan V, Karnik ND. Antioxidant status in patients with acute myocardial infarction. *Indian J Clin Biochem*. 2007;22:45–51.

44. Jia Y, Chang HC, Schipma MJ, Liu J, Shete V, Liu N, Sato T, Thorp EB, Barger PM, Zhu YJ, et al. Cardiomyocyte-specific ablation of Med1 subunit of the mediator complex causes lethal dilated cardiomyopathy in mice. *PLoS One*. 2016;11:e0160755.

45. Krebs P, Fan W, Chen YH, Tobita K, Downes MR, Wood MR, Sun L, Li X, Xia Y, Ding N, et al. Lethal mitochondrial cardiomyopathy in a hypomorphic Med30 mouse mutant is ameliorated by ketogenic diet. *Proc Natl Acad Sci USA*. 2011;108:19678–19682.

46. Lou X, Burrows JT, Scott IC. Med14 cooperates with brg1 in the differentiation of skeletogenic neural crest. *BMC Dev Biol*. 2015;15:41.

47. Rocha PP, Scholze M, Bleiss W, Schrewe H. Med12 is essential for early mouse development and for canonical Wnt and Wnt/PCP signaling. *Development*. 2010;137:2723–2731.

48. Trehan A, Brady JM, Maduro V, Bone WP, Huang Y, Golas GA, Kane MS, Lee PR, Thurm A, Gropman AL, et al. Med23-associated intellectual disability in a non-consanguineous family. *Am J Med Genet A*. 2015;167:1374–1380.

49. Kasahara A, Cipolat S, Chen Y, Dorn GW II, Scorrano L. Mitochondrial fusion directs cardiomyocyte differentiation via calcineurin and notch signaling. *Science*. 2013;342:734–737.

50. Song M, Franco A, Fleischer JA, Zhang L, Dorn GW II. Abrogating mitochondrial dynamics in mouse hearts accelerates mitochondrial senescence. *Cell Metab*. 2017;26:872–883.e875

51. Li H, Lahti JM, Valentine M, Saito M, Reed SI, Look AT, Kidd VJ. Molecular cloning and chromosomal localization of the human cyclin C (CCNC) and cyclin E (CCNE) genes: deletion of the CCNC Gene in human tumors. *Genomics*. 1996;32:253–259.

52. Bozickovic O, Hoang T, Fenne IS, Helland T, Skartveit L, Ouchida M, Mellgren G, Sagen JV. Cyclin C interacts with steroid receptor coactivator 2 and upregulates cell cycle genes in MCF-7 cells. *Biochim Biophys Acta*. 2015;1853:2383–2391.

SUPPLEMENTAL MATERIAL

Data S1.

Expanded Methods

Mouse models: Cardiomyocyte-specific cyclin C-knockout mice: Cyclin C floxed mice (cyclin C fl/fl) were kindly provided by Dr. Peter Sicinski (Harvard University) and cyclin C cardiac-specific knockout (cKO) mice were generated by breeding cyclin Cfl/fl mice with C57/BL6 transgenic mice containing the α-myosin heavy chain (α-MHC) promoter-driven cre recombinase to establish heterozygous cyclin Cfl/+;αMHC-Cre mice. Male cyclin $C^{fl/+}$-αMHC Cre+ mice were bred to female cyclin C fl/fl mice to establish homozygous cyclin C fl/fl; αMHC Cre/+. Studies were done using Cre-negative cyclin C fl/fl littermates as controls.

Conditional cardiomyocyte-specific cyclin C-overexpressing mice were generated by the University of Iowa Genome Editing Facility by pronuclear injection of a linearized targeting vector into B6 × SJL F2 eggs. The targeting construct was made by replacing the ZsGreen coding sequence of pCAG-loxPSTOPloxP-ZsGreen (Addgene #51269) with the coding region of *CCNC* (NCBI accession NM_005190) containing a C-terminal Myc tag. Founders were identified by genotyping with primers specific for the hGH polyA sequence downstream of *CCNC* (forward, 5′-GTCTATTCGGGAACCAAGCTGGAGT-3′; reverse, 5′-AACAGGCATCTACTGAGTGGACCCAA-3′) and backcrossed to C57BL/6 mice (Charles River Laboratories, strain code 027) for at least 5 generations for all studies. Cyclin C overexpression was induced through crossing loxPSTOPLoxP-*CCNC* mice with αMHC-Cre expressing mice. Unless otherwise stated, at least 3 transgenic (fl/+; Cre+) and 3 fl/+ littermate control mice were used for all experiments. Similar results were obtained between male and female animals. Age-matched cyclin C fl/+; Cre negative and Myh6-Cre alone were used as

controls. Animals were fed standard chow and water given ad libitum. All experimental procedures were approved by the University of Iowa Animal Care and Use Committee.

Human explanted heart specimen procurement: The human explanted heart samples were collected under the protocols approved by the Health Research Ethics Board of the University of Alberta. Signed consent and assent were obtained from individual participant (or next of kin) prior to cardiac transplantation or organ donation. Non-failing myocardial specimens were procured from n=5 consecutive donors with no cardiovascular history who were unsuitable for transplant due to medical or technical issues, such as ABO blood type incompatibility, as per Human Organ Procurement and Exchange Program at the University of Alberta Hospital. Adult failing heart tissues were collected from patients with end-stage heart failure secondary to ischemic coronary artery diseases (n=6) as part of the Human Explanted Heart Program at the Mazankowski Alberta Heart Institute. The collections were conducted when the patients underwent cardiac transplantations, and all myocardium samples were excised from the post-MI left ventricular free wall avoiding epicardial adipose tissue within 5-10 minutes of its excision following cold cardioplegia. The samples were immediately flash-frozen in liquid nitrogen and later stored in ultra-low (-80℃) freezers. Detailed demographic and clinical profile of all patients with coronary artery diseases are summarized in **Table 1**. The non-failing control group consisted of n=5 explanted hearts from males with a median age 52 years (IQR 38.0–54.0 years) and median LVEF of 60% (IQR 60-65%).

Cell culture: To isolate primary cultures of neonatal rat cardiomyocytes (NRCM), hearts from P3 Wistar rats (Jackson labs) were rapidly excised and washed in chilled Hanks Balanced Salt Solution (HBSS, 1X). The atria were removed and ventricles carefully minced and dissociated into single cells by proteolytic enzymes (Pierce Primary Cardiomyocyte Isolation Kit) dissolved

in HBSS in a 37°C incubator for 30-35 min with gentle stirring. Enzymes were removed and cells were washed 3 times with chilled HBSS. To breakup tissue, cells were gently pipetted repeatedly with L- Dulbecco's modified Eagle's medium DMEM (M199, 10% horse serum, 5% fetal bovine serum, 1% penicillin). Cells were plated onto collagen-coated culture plates and allowed to adhere to the plates for 24 hours before changing to basic experimental culture DMEM media (M199, 2% fetal bovine serum, 1% penicillin). NRCMs were stressed with Angiotensin II (100 nM, Sigma), Isoproteonol (200 nM, Sigma) or palmitate (50 µM, Sigma) 48 hours post seeding for varied durations. The culture medium was changed daily until the cells were harvested.

Adeno-associated virus expression: Primary NRCM were plated onto collagen-coated (BD Biosciences) coverslips and maintained in modified DMEM culture (Pierce Primary Cardiomyocyte Isolation DMEM cell culture) medium for 24 hours. Cells were infected with adeno-associated virus (5×10^7 vg/uL) containing cDNA for wild type cyclin C, mutant cyclin C-HAD, mutant cyclin C-ND, or GFP (empty vector control) for 72 hours. Adeno-associated vectors were generated by the University of Iowa Gene Vector Core Facility.

Cellular and whole heart lysate fractionation: Following treatment, cells were collected and fractionation was completed using the NE-PER Nuclear and Cytoplasmic Extraction kit (Thermo) according the manufacturer's instructions. Cells and tissue were washed with chilled PBS and centrifuged at 500xg for 5 minutes. Supernatant was discarded; cytoplasmic and nuclear proteins were extracted and stored at -80°C degrees. Equal protein amounts from each fraction were analyzed by Western blotting.

Quantitative real-time PCR (qRT-PCR): Ventricular tissue was isolated and flash frozen in liquid nitrogen and stored at −80°C until processed. Flash frozen ventricles were pulverized with

a Bessman tissue pulverizer before homogenization. Total RNA was extracted in TRIzol reagent (Invitrogen) using a Postter- elvehjem tissue grinder. Reverse transcriptase-PCR was performed to generate cDNA using SuperScript-III (Invitrogen). For qRT-PCR, 50 ng of cDNA were used for each reaction with iTAQ Universal Sybergreen reagent (BioRad) using the QuantStudio 6 Flex system (Applied Biosystems). Gene expression was analyzed using the ΔΔCT method and relative expression was normalized to Rpl7l1. Sequences for the primers are as listed in previous studies[1, 2].

Immunofluorescence microscopy: Isolated NRCMs were grown on collagen-coated glass coverslips. After treatment, cells were washed 3 times with PBS and fixed with ice cold ethanol (100% v/v) for 15 minutes at room temperature. To suppress unspecific labeling, cells were incubated with blocking solution (1% BSA, 1% goat serum, and 0.1% Triton X-100 in PBS) for 1 hour at room temperature. Rabbit anti-Cyclin C (1:100, Bethyl, Thermo) antibody, Mitotracker orange (1:500, Sigma) and Phallodin-647 (1:400, Life Technologies) in 1% BSA solution (in PBS, pH 7.4) were added for 1 hour at room temperature. After three washes with chilled PBS the secondary antibodies conjugated with Alexa Flour 488 or Alexa Flour 568 (1:300) were added for 1 hour at room temperature. Cells were washed and mounted with vecta shield (Vectorlabs) containing DAPI for nuclear staining. Immunofluorescence was observed using a Zeiss 710 confocal microscope. Whole hearts are harvested, paraffin-embedded, and cut into 10μm sections with a rotary microtome (Leica). Following dewaxing, rehydration and antigen retrieval, sections are incubated with blocking solution (0.1% TBS/T / 10% goat serum; 30 minutes at room temperature), followed by incubation with primary antibody (Ab°) either overnight at 4 °C or 1–2 hours at room temperature and secondary antibodies conjugated to either Alexa 488 or Alexa 594 (Life Technologies) for two hours at room temperature. Fluorescent

slides are washed, then mounted with Vectashield Mounting medium with DAPI (Vector Labs). Immunofluorescence is observed using a Zeiss 710 confocal microscope.

Immunohistochemical staining: All samples were processed in consultation with the University of Iowa Central Microscopy Facility and Comparative Pathology core. Briefly, hearts were fixed in 4% paraformaldehyde, paraffin embedded and sectioned (10μm) using a standard microtome. Heart sectioned were deparaffinized and stained to determine changes in morphology (hematoxylin and eosin (H&E)) and fibrosis (Masson's trichrome) as previously published[1, 2].

Immunoloblot analysis: Isolated NRCM were removed from plates with 0.25% Trypsin in 37°C incubator for 3-5 min. Cells were washed twice with PBS and centrifuged at 30,000xg for 10 minutes. Whole hearts were harvested and rinsed with chilled PBS. Ventricles were flash frozen and kept at –80°C until processing for total protein. Ventricular tissue was pulverized with a Bessman tissue pulverizer (Spectrum Labs) and homogenized in RIPA buffer (25 mM Tris-HCl pH 7.6, 150 mM NaCl, 1% NP-40, 1% Na-deoxycholate, 0.1% SDS; Thermo Fisher Scientific) containing cOmplete Mini protease and phosphatase inhibitors (Roche). Cells or tissue samples were sonicated on ice for 10 seconds with an ultrasonic liquid processor (Qsonica) and centrifuged at 20,000 g at 4°C. Protein concentrations were determined by the bicinchoninic acid assay method (Thermo Fisher Scientific). Samples were separate for immunodetection using standard sodium dodecyl sulfate–polyacrylamide gel electrophoresis (SDS-PAGE) using 20 μg lysate per lane was separated on 4%–20% Tris-glycine SDS gels (Bio-Rad Laboratories) and transferred to 0.45 μm polyvinyl difluoride membranes (EMD Millipore). Membranes were blocked in blocking buffer (10 mM Tris-HCl pH7.4, 150 mM NaCl, 0.05% Tween-20, 5% BSA or 5% nonfat dry milk), incubated in blocking buffer with primary antibodies overnight at 4°C, washed, and incubated with HRP-linked secondary antibodies (Jackson ImmunoResearch at

1:10,000) for 1 hour at room temperature. Primary antibodies were used at the following

dilutions: Cyclin C (anti-rabbit, Bethyl, 1:2,000; Thermo, 1:1000), Drp1 (anti-rabbit, Cell

Signaling, 1:500), pDrp1(616) (anti-rabbit, Cell Signaling (1:500), anti-rabbit, cytochrome C

(Cell Signaling (1:1000). Gapdh (Cell Signaling 2118, 1:8,000), Topo-isomerase (Cell Signaling

1:500) and RNA-pol II (Sigma A7811, 1:10,000) were used as loading control.

Mitochondria respiration analysis: Complex activity was assessed using a Seahorse XF96

Extracellular Flux Analyzer by the University of Iowa Free Radical and Radiation Biology

Research Core, following a protocol previously established[3, 4]. NRCM's were isolated and plated

at 40,000 cells was loaded per well in the XF96 plate format and treated with Cyclin CAAV for

72 hours. Plates were spun at 4 °C at 2000 g for 20 minutes to affix cells to the wells. The assay

was run in the presence of 5 mM pyruvate and 5 mM malate, with sequential injections of FCCP

and Antimycin A to final concentrations of 4 μM apiece. A minimum of 7 technical replicates

was used for each cell isolation and treatment. Statistical analysis was accomplished using

Microsoft Excel.

The Oxygraph-2k (O2k, OROBOROS Instruments, Innsbruck, Austria) was used for

measurements of respiration and combined with the Fluorescence-Sensor Green of the O2k-Fluo

LED2-Module for H_2O_2 measurement at the University of Iowa Metabolic Core. Two O2k

instruments were used in parallel. Experiments using tissue homogenate and permeabilized cells

were performed in MiR05 (110 mM sucrose, 60 mM K-lactobionate, 0.5 mM EGTA, 3 mM

$MgCl_2$, 20 mM taurine, 10 mM KH_2PO_4, 20 mM HEPES, pH 7.1 at 30 °C, and 0.1% BSA

essentially fatty acid free). Dulbecco's modified eagle medium supplemented with 10% fetal

bovine serum and 50 units/mL penicillin and 50 μg/mL streptomycin was used for measurements

on intact cells. All experiments were performed at 37 °C. The medium was reoxygenated when oxygen concentrations reached 80 µM.

Myocardial infarction surgeries: MI induction was performed as described[5]. Briefly, the mouse was placed in a supine position before intubation and ventilation as previously described using a rodent miniventilator (Harvard Apparatus, Hollston, MA) hooked up to an oxygen concentrator apparatus Millenium (Respironics, Marietta, GA) that provided 94–98% oxygen. The ventilator was set at positive end-expiratory pressure (PEEP) mode of ventilation with a stroke volume of 200 Al and at 200 strokes per minute. Surgery was performed using a Leica MZ 12 microscope. The left pectoralis major muscles were refracted towards the right shoulder and the left rectus thoracis and serratus anterior muscles were reflected towards the left with two hooked microretractors. The third intercostal space was exposed and delicately dissected 3 mm from the sterno–costal junction, avoiding injury to the left internal mammary artery. Thoracotomy proceeded laterally on the upper border of the fourth rib to avoid damaging the intercostal nerves and vessels on the lower border of the third rib. A 10/0 Prolene suture (Ethicon, Johnson & Johnson, Brussels, Belgium) was then passed under the LAD at 1 mm distal to left atrial appendage, immediately after the bifurcation of major left coronary artery. The chest wall was closed by approximating the third and fourth ribs with one or two interrupted stitch using a 5/0 Chromic Catgut absorbable suture (Ethicon, Johnson & Johnson, Brussels, Belgium). Skin closed with 6/0 Prolene continuous sutures. The mouse was gently disconnected from the ventilator and spontaneous breathing should resume almost immediately.

Ischemic reperfusion surgeries: Ischemia induction was performed as described[5]. Following 20 minutes of ischemia, the 10/0 prolene suture was removed to allow for reperfusion of the ischemic area and generation of I/R injury for 90 minutes. Next, the LAD was relegated and 2% Evans blue

was directly injected into aorta to observe ischemic and remote regions, which were immediately harvested. Throughout the process, similar intubation and ventilation processes were used as previously described for the MI procedure.

Cardiac function analysis: To identify potential changes in gross cardiac morphology and markers of heart failure, body weight (g), heart weight (ventricle and atria) and lung weight (mg) were measured. In order to determine and evaluate the degree of infarction, we used triphenyl tetrazolium chloride (TTC) staining on transverse heart sections. Sections will were incubated in 1% TTC in PBS for 20 min at 37 °C and fixed in 10% formalin overnight. The samples were imaged using a Leica MZ 12 dissection scope. Cardiac function was evaluated in conscious mice in the University of Iowa Cardiology animal phenotyping core laboratory. Left-sided chest hair was removed. Parasternal long and short axis views were obtained using a high-frequency echocardiography (30 MHz) linear array transducer (Vevo 2100; Visual Sonics). Measurements performed were done by a single experienced operator blinded to the mouse genotypes.

RNA sequencing analysis: The University of Iowa Institute of Human Genetics, Genomics Division, generated polyA-enriched stranded RNA libraries followed by RNAseq using the Illumina HiSeq platform. Raw sequence reads were analyzed with BaseSpace (www.illumina.com) by aligning reads to the Mus musculus mm10 genome using the TopHat Alignment app. Transcripts were assembled and significant differentially expressed genes were determined with the Cufflinks Assembly and DE app using a false discovery rate <0.05.

RNA-seq analysis list of differentially regulated genes significantly changed between cyclin C fl/fl and cyclin C cKO mouse hearts was entered into the PANTHER classification system (Pantherdb.org). Classification of data was compiled via Biological Process and a Pie Chart was created. Alterations in Biological Processes pertaining to Metabolic Processes was

performed to break down individual metabolic processes. RNA-seq analysis data was uploaded to Qiagen's Ingenuity Pathway Analysis (IPA; Valencia, CA) and biological and interaction networks were generated. The gene list was analyzed for biological function enrichment analysis, upstream regulator analysis, and networks of interaction between molecules algorithmically generated based on their connectivity.

High magnification transmission electron microscopy: Jeol electron microscope (JEM-1230) was used at 1,500x-30,000x direct magnifications (Jeol) on 90-nm sections of fixed left ventricular tissue or AAR regions of sham or I/R treated hearts. All samples were processed in consultation with the University of Iowa Central Microscopy Facility. Tissue was fixed in 2% glutaraldehyde and 2% paraformaldehyde in 0.1M buffer, dehydrated and embedded in resin bead capsules and baked (70°C oven) for 24 hrs. Tissue was sectioned (0.9 µm thickness, Leica UC6 ultramicrotome II), on 300 µm mesh copper grids, stained using NaOH and lead citrate, and imaged. Mitochondrial size, area and length were measured using ImageJ in a double blind study. Analysis was performed using Matlab software. Briefly, mitochondrial length and area were binned, normalized to compute percentages and then plotted via histogram. Unbinned data was fit to a gamma distribution curve. Statistical analysis was performed using Kruskal Wallis to detect changes in distribution and a student T-test to detect changes in the mean.

Pharmacological studies: *In vitro* analysis: Isolated P3 NRCM was treated with the Cdk1 inhibitor, Roscovitine (R7772 SIGMA, MO): 5 µM, 6 hour treatment; NU6102 (CAS 444722-95-6, Sigma, MO): 5 µM, 6hour. *In vivo* analysis: Roscovitine (R7772 SIGMA MO) is solubilized in DMSO (Sigma, St. Louis, MO) and diluted in 0.9% sodium chloride. Intraperitoneal injection of Roscovitine was performed 1hour before ischemic reperfusion surgery.

Coimmunoprecipiation (Co-IP): The AAR region of ventricular lysates were harvested from 8-10 week old C57/bl-6 mice treated with sham or I/R surgeries and prepared using RIPA buffer with the addition of protease phosphatase inhibitor cocktail (Roche). Co-immunoprecipitation was performed using the Dynabead Protein A protocol (Thermo fisher, 10002D) and preformed according to manufacturer's instructions. Briefly, Dynabeads were prepared and bound to 10 µg of Cdk1 (Santa cruz) or cyclin C antibody (Thermo) in 200 µL PBS with Tween-20, incubated for 20 minutes at room temperature. To the extracts, 5 µl of cyclin C (Thermo) or Cdk1(Santa cruz) antibody was added and incubated with gentle rotation for 2 hours at 4°C followed by the addition of 5 µl of Dynabeads Protein A (Invitrogen) with a further incubation of 1 to 2 hours. Immune complexes were washed, target antigen was eluted and gently resuspended in NuPAGE 4X LDS Sample Buffer (Thermo) and NuPAGE 10X Sample Reducing Agent (Thermo) and detected via immunoblotting in the presence of cyclin C(Thermo) or Cdk1 (Santa Cruz) antibodies.

Table S1. Baseline clinical characteristics of human explanted heart specimen.

	Coronary Artery Diseases Median (IQR)
Demographic	
No. of Patients studied	6
Age at transplant (years)	56.0 (47.8-60.5)
Sex (Male)	6/6
Anthropometric	
Weight (kg)	85.0 (83.6-94.3)
Height (m)	1.8 (1.7-1.8)
BMI (kg/m^2)	28.2 (25.3-32.1)
Physical assessment	
HR (bpm)	83.0 (77.0-100.0)
SBP (mmHg)	116.0 (95.5-142.5)
DBP (mmHg)	70.0 (67.0-70.8)
NYHA (Class I/II/III/III)	0/0/0/6
Comorbidities (%)	
COPD/Asthma	1/6
DM	1/6
Dyslipidemia	2/6
Kidney disease	2/6
HTN	2/6
Obesity	4/6
Other diseases	4/6
History	
Smoking	4/6
Alcoholic	0/6
Echocardiography	
LVEF (%)	20.1 (17.5-22.7)
LVEDD (mm)	55.5 (53.5-58.8)
LVESD (mm)	39.0 (34.5-51.0)
Blood Parameters	
Hemoglobin (g/L)	112.0 (93.5-135.0)
WBC (10^9/L)	7.8 (6.3-9.1)
BNP (pg/ml)	973.0 (747.5-986.5)
Creatinine (μmole/L)	97.5 (84.3-110.8)
eGFR (ml/min/1.73m^2)	71.5 (63.5-95.3)
Devices	
Pacemaker	1/6
ICD	1/6
BiV-ICD	1/6
VAD	4/6
Medications	

|	
ACEi/ARB	4/6
Beta Blocker	3/6
Diuretics	4/6
Anti-coagulation	3/6
Statin	3/6
PPI	2/6
Anti-arrhythmic	2/6
Vitamin D	1/6

BMI = body mass index; HR = heart rate; SBP = systolic blood pressure; DBP = diastolic blood pressure; NYHA = New York Heart Association; COPD = chronic obstructive pulmonary disease; LVEF = LV ejection fraction; LVEDD = LV end diastolic diameter; LVESD = LV end systolic diameter; WBC = white blood cell; eGFR = estimated GFR based on the MDRD equation; ICD = implantable cardioverter-defibrillator; BiV-ICD = biventricular implantable cardioverter-defibrillators; VAD = ventricular assist device; ACEi = angiotensin-converting enzyme inhibitor; ARB = angiotensin receptor blocker; PPI = proton pump inhibitor. Available data are presented as medians (with lower and upper quartiles) or numbers, where appropriate.

**Figure S1. Developmental cyclin C expression, cyclin C cTg histology and MI pathology data.**
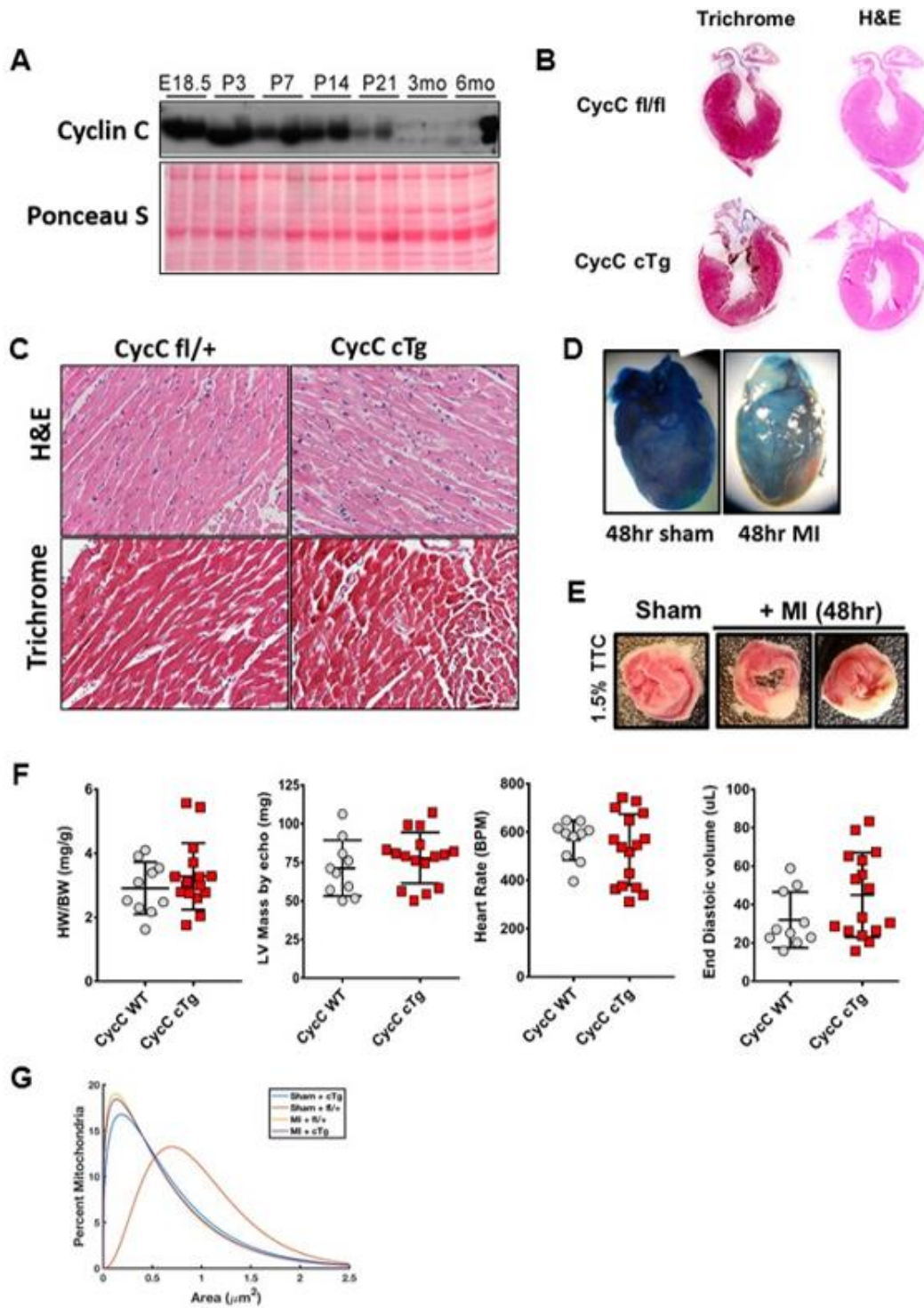
(A) Immunoblotting of cyclin C and Ponceau S protein stain in mouse heart tissues from time periods embryonic day (E)18.5, postnatal day (P)3, P7, P14, P21, 3 month, 6 month. **(B)** Representative heart sections of 12-wk old cyclin C cTg and fl/fl control mice stained with Masson's trichrome and hematoxylin and eosin (H&E) for morphological and fibrotic analysis. **(C)** Histological images of paraffin embedded samples stained using (H&E) and Masson's trichrome in 12-wk old Cyclin C cTg and fl/+ controls. **(D)** Gross hearts stained with Evans blue dye of 8 wk-C57/bl6 mice following 48hr sham or myocardial surgery. **(E)** Heart sections stained with 1.5% 2,3,5 triphenyltetrazolium chloride (TTC) of 8 wk-C57/bl6 mice following 48hr sham or myocardial surgery. **(F)** Heart weight to body weight ratios, ventricular mass, heart rate and end diastolic volume for cyclin C cTg and fl/+ controls. **(G)** Cumulative mitochondrial area distribution from cyclin C cTg and fl/+ controls with or without MI.

Figure S2. Ablation of cardiac cyclin C results in increased heart and lung mass and altered gene expression.
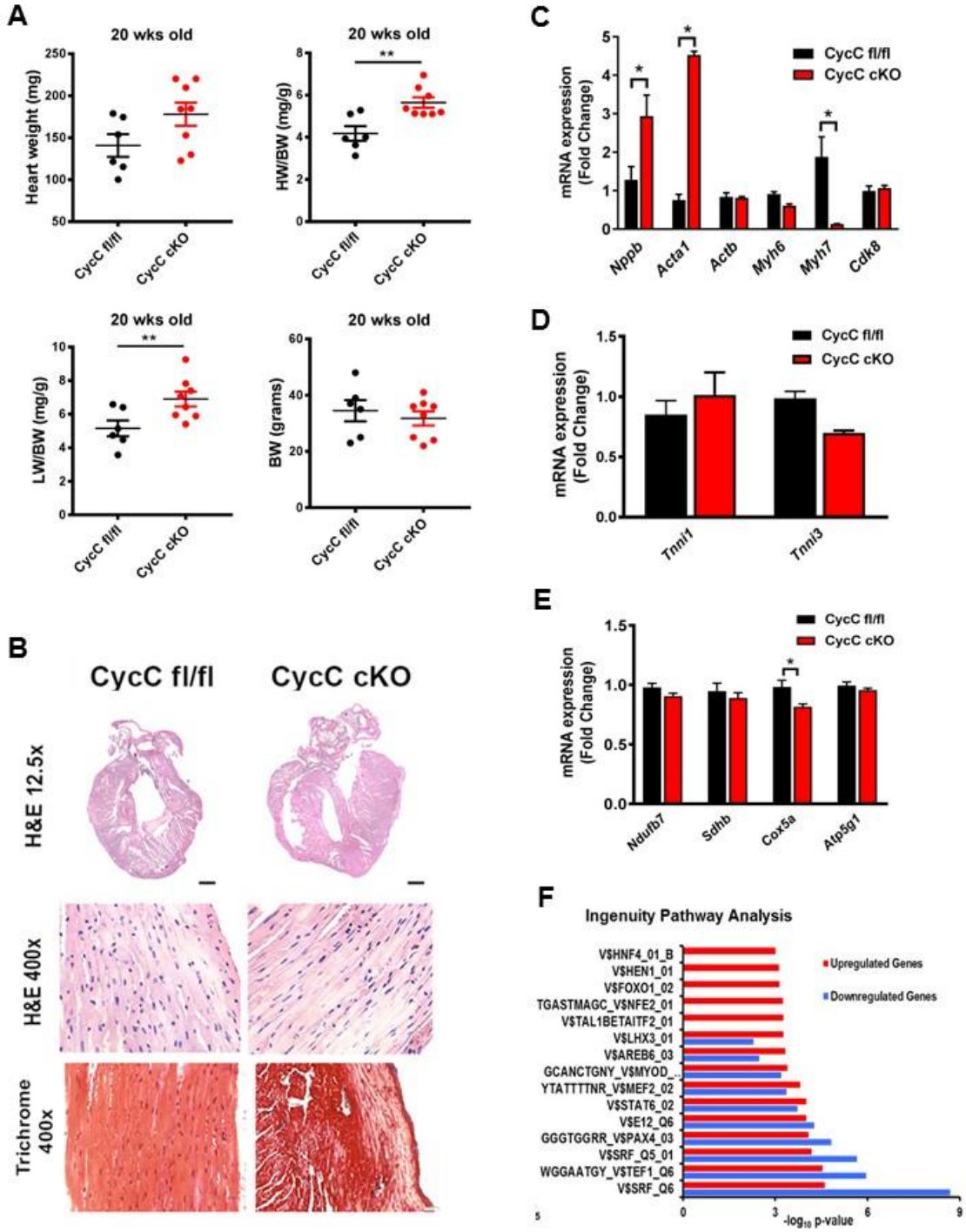
(A) Whole heart, body, and lung weights of 20-wk old cyclin C cKO and fl/fl controls. Data are means ± SE (n=6-10), **P < 0.05. **(B)** Representative heart sections and histological images of paraffin-embedded 12-wk old cyclin C cKO and fl/fl control mice stained with Masson's trichrome and hematoxylin and eosin (H&E) for morphological and fibrotic analysis. Scale bars; 0.5mm. **(D-E)** mRNA expression of (c) *Cdk8* and markers of cardiac failure (*Nppb, Acta1, Actb, Myh6, and Myh7),* (d) cardiac-specific genes (*Tnni1, Tnni3*), and (e) genes involved in metabolism *(Ndufb7, Sdhb, Cox5a, Atp5g1*) in ventricular tissue from 6-wk old cyclin C cKO and control hearts. **(F)** Enriched transcription factor binding motifs identified in the promoters of >1.5-fold upregulated (red) and >1.5-fold downregulated (blue) differentially expressed genes from RNA-seq results using WebGestalt tool.

Figure S3. Adult cardiomyocyte mitochondrial morphology is sensitive to stress and dependent on cyclin C and Cdk1.
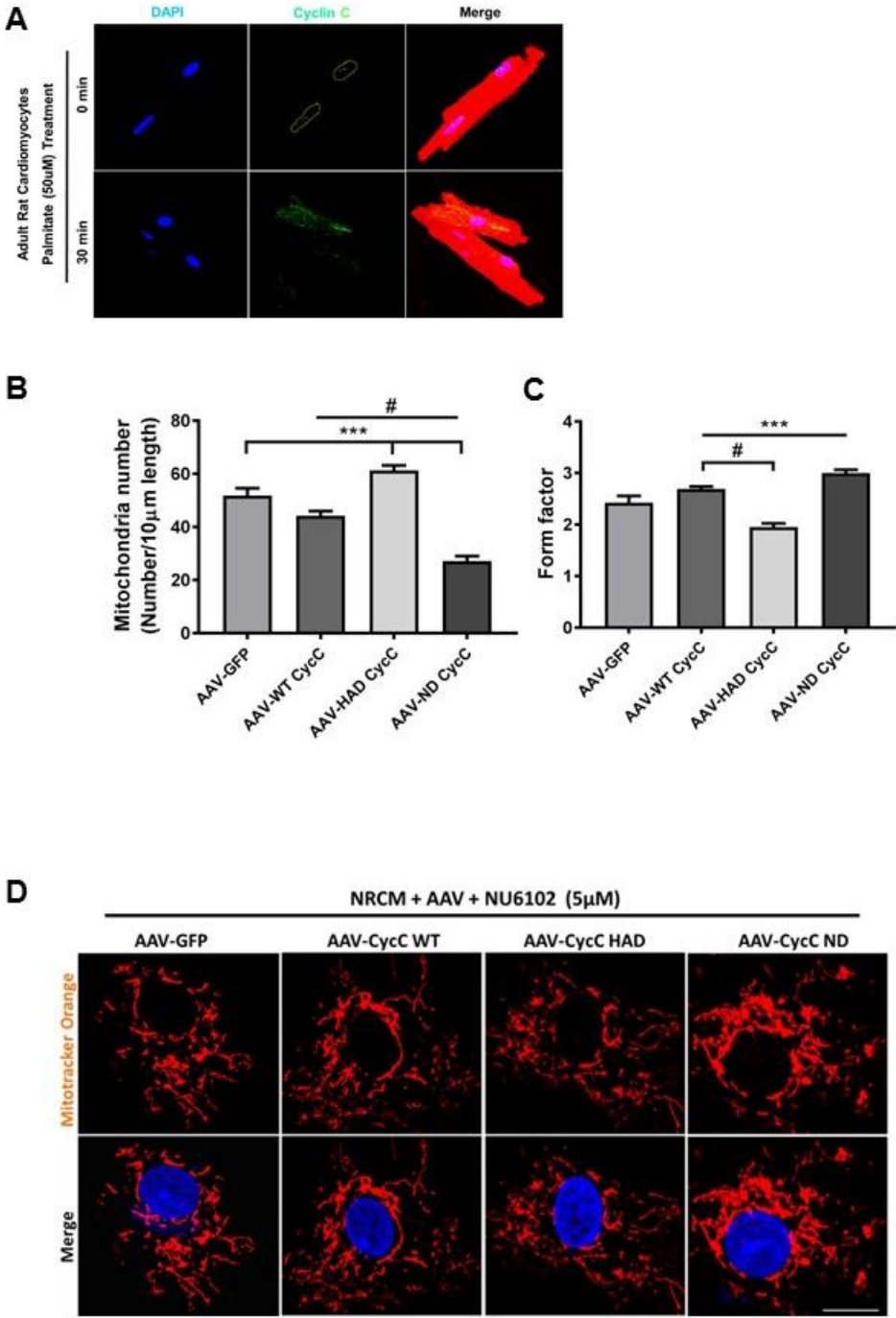
(A) Immunofluorescence (IF) analysis of cyclin C (green) and α-actinin (red) in cardiomyocytes isolated from 8-wk old adult rats with and without palmitate treatment (50 µM, 30 min). **(B-C)** Mitochondrial number (c), form factor (d) and overall morphology (e) of NRCMs 72 hours after transduction with indicated AAV's using Image J processing program. (***$P<0.05$; # = $P<0.05$; ANOVA, n> 400 cells counted, N=5). In **(D),** cells were treated with the Cdk1 inhibitor, NU6102 (5µM, 1hr) prior to staining nuclei with DAPI (blue) and mitochondria (red) with Mitotracker orange (200 nM).

Supplemental References:

1. Hall DD, Ponce JM, Chen B, Spitler KM, Alexia A, Oudit GY, Song LS, Grueter CE. Ectopic expression of cdk8 induces eccentric hypertrophy and heart failure. *JCI Insight*. 2017;2

2. Spitler KM, Ponce JM, Oudit GY, Hall DD, Grueter CE. Cardiac med1 deletion promotes early lethality, cardiac remodeling, and transcriptional reprogramming. *Am J Physiol Heart Circ Physiol*. 2017;312:H768-H780

3. Pereira RO, Tadinada SM, Zasadny FM, Oliveira KJ, Pires KMP, Olvera A, Jeffers J, Souvenir R, McGlauflin R, Seei A, Funari T, Sesaki H, Potthoff MJ, Adams CM, Anderson EJ, Abel ED. Opa1 deficiency promotes secretion of fgf21 from muscle that prevents obesity and insulin resistance. *The EMBO journal*. 2017;36:2126-2145

4. Anderson EJ, Kypson AP, Rodriguez E, Anderson CA, Lehr EJ, Neufer PD. Substrate-specific derangements in mitochondrial metabolism and redox balance in the atrium of the type 2 diabetic human heart. *Journal of the American College of Cardiology*. 2009;54:1891-1898

5. Gao E, Lei YH, Shang X, Huang ZM, Zuo L, Boucher M, Fan Q, Chuprun JK, Ma XL, Koch WJ. A novel and efficient model of coronary artery ligation and myocardial infarction in the mouse. *Circ Res*. 2010;107:1445-1453